UNIVERSIDADE FEDERAL DE PERNAMBUCO
DEPARTAMENTO DE FÍSICA
PROGRAMA DE PÓS-GRADUAÇÃO EM FÍSICA

LUAN MARTINS TORRES DE MORAES

CORRELATED DISORDER-DRIVEN SUPERCONDUCTIVITY IN QUASI-1D SAMPLES

Recife

2023

LUAN MARTINS TORRES DE MORAES

CORRELATED DISORDER-DRIVEN SUPERCONDUCTIVITY IN QUASI-1D SAMPLES

Dissertation presented to the Posgraduate program of the Physics Department of the Federal University of Pernambuco as partial requirement to obtain the degree of Master in Physics.

Program of Studies: Física da Matéria Condensada e de Materiais

Advisor: José Albino Oliveira de Aguiar

co-Advisor: Mihail D. Croitoru

Recife

2023

Catalogação na fonte
Bibliotecária Nataly Soares Leite Moro, CRB4-1722

M828c Moraes, Luan Martins Torres de
Correlated disorder-driven superconductivity in quasi-1d samples / Luan Martins Torres de Moraes. – 2023.
80 f.: il., fig.

Orientador: José Albino Oliveira de Aguiar.
Dissertação (Mestrado) – Universidade Federal de Pernambuco. CCEN, Física, Recife, 2023.
Inclui referências.

1. Física da matéria condensada e de materiais. 2. Desordem correlacionada. 3. Supercondutividade. 4. Amostras quase 1D. 5. Intensidade da desordem. 6. Correlações espaciais. I. Aguiar, José Albino Oliveira de (orientador). II. Título.

530.41 CDD (23. ed.) UFPE- CCEN 2023 - 123

LUAN MARTINS TORRES DE MORAES

CORRELATED DISORDER-DRIVEN SUPERCONDUCTIVITY IN QUASI-1D SAMPLES

Dissertação apresentada ao Programa de Pós-Graduação em Física da Universidade Federal de Pernambuco, como requisito parcial para a obtenção do título de Mestre em Física.

Aprovada em: 31/07/2023.

BANCA EXAMINADORA

_____

Prof. Dr. José Albino Oliveira de Aguiar
Orientador
Universidade Federal de Pernambuco

_____

Prof. Dr. Renê Rodrigues Montenegro Filho
Examinador Interno
Universidade Federal de Pernambuco

_____

Prof. Dr. Andrey Chaves
Examinador Externo
Universidade Federal do Ceará

There was a time when darkness covered the entire earth, where threat permeated all that was alive. During this time, a great light appeared, driving the demons far beyond familiar places. However, they still linger there, waiting for this mere flame to extinguish and return to their place of origin: our minds. I dedicate this thesis to all those who, in some way, fight for the preservation of this light.

ACKNOWLEDGEMENTS

I would like to thank my parents, Alexandre and Dulce, for raising me, providing me with a proper education, and supporting my academic journey.

I am grateful to all my friends who have been part of this journey since my early education, but I would like to mention some who were particularly important during my master's degree: Diego Bruno, Emanuel Pinheiro, Irio Coutinho, Jefferson Deyvis, José Jailson, Larissa Faneco, Maria Inês, Michel Arruda, Vinicius Farah, and Yuri Falcão. Each of you has been instrumental to me during this journey, and some of you have been so essential that I considered thanking you individually, but I believe it would be potentially more unfair than I already am by mentioning you directly.

To the Physics professors at UFRPE and UFPE, Antônio Murilo, Pedro Hugo, and Raul Montagne, who, in my opinion, have been the greatest contributors to the excellent education I received.

To the Mathematics professors at UFRPE, Lorena Brizza and Thiago Mendonça, not only for providing me with a solid foundation in mathematics but also for the years of friendship that have endured even after classes ended.

To my faithful high school friends, Breno Italo, George Henrique, Lincoln Cavalcante, and Yuri Barcelar. I am truly grateful that you have been with me until today, and we always have a great time together.

To all the members of the Pinto family, who practically adopted me as one of their own: Andrea, Bianca, Bruno, Eduarda, Eduardo, Felipe, and Luciana. I am deeply grateful to all of you for providing me with shelter when I needed it throughout all these years.

To my martial arts instructor, Cleiton Rodrigo, who not only taught me to be stronger but also taught me to approach life with greater lightness.

To my advisors, José Albino Aguiar and Mihail Croitoru, for their guidance and the opportunities they provided.

To CAPES, UFPE, and CETENE for granting me the master's scholarship and for providing computational resources.

Lastly, to my grandmother, who may no longer be with us, but I feel that she continues to watch over me, even from a distance.

ABSTRACT

The recent surge of interest in the interplay between disorder and superconductivity has witnessed significant advancements in theory and experiment. While prior research mainly focused on disorder strength's impact, recent studies show disorder can remarkably enhance superconductivity. Structural disorder has led to notable improvements in superconducting characteristics, exemplified by MoSe chains with Na atoms (PETROVIC et al., 2016) and TaS_2 monolayers (PENG et al., 2018). However, current disorder models lack consideration for spatial correlations, which are prevalent in real systems. Long-range correlations, as demonstrated in zero-temperature superconducting studies (NEVEROV et al., 2022), alter statistical properties of the order parameter, reinforcing superconducting correlations against disorder. This dissertation explores correlated disorder's effect on nanowire superconductivity, revealing intricate connections between electron density, disorder, correlations, and sample dimensions. Specifically, electron density modulates order parameter dependence on transverse dimensions, showing weakened quantum-size effects near the mid-band. Disorder's influence varies with electron density; mid-band exhibits milder disorder impact than band edges. In high electron density, weak correlation-dependent OP increase is noted with size reduction, contrasting the low-density regime where a strong, non-monotonic correlation-dependent increase emerges. This research emphasizes correlation's vital role in robust superconductivity, offering tailored material design opportunities.

Keywords: correlated disorder; superconductivity; quasi-1D samples; disorder strength; spatial correlations.

RESUMO

O recente aumento significativo do interesse na interação entre desordem e supercondutividade tem testemunhado avanços significativos na teoria e experimentação. Enquanto pesquisas anteriores focaram principalmente no impacto da intensidade da desordem, estudos recentes mostram que a desordem pode notavelmente aprimorar a supercondutividade. A desordem estrutural tem levado a melhorias notáveis nas características supercondutoras, exemplificadas pelas cadeias de MoSe com átomos de Na (PETROVIC et al., 2016) e monocamadas de TaS_2 (PENG et al., 2018). No entanto, os modelos atuais de desordem não consideram as correlações espaciais, que são prevalentes em sistemas reais. Correlações de longo alcance, como demonstrado em estudos de supercondutividade a zero temperatura (NEVEROV et al., 2022), alteram as propriedades estatísticas do parâmetro de ordem, fortalecendo as correlações supercondutoras contra a desordem. Esta dissertação explora o efeito da desordem correlacionada na supercondutividade de nanofios, revelando conexões intrincadas entre densidade de elétrons, desordem, correlações e dimensões da amostra. Especificamente, a densidade de elétrons influencia a dependência do parâmetro de ordem nas dimensões transversais, mostrando efeitos de tamanho quântico enfraquecidos perto da banda média. A influência da desordem varia com a densidade de elétrons; a banda média exibe impacto de desordem mais suave do que as bordas da banda. Na alta densidade de elétrons, um fraco aumento dependente da correlação no parâmetro de ordem é observado com a redução do tamanho, contrastando com o regime de baixa densidade, onde um forte aumento dependente da correlação e não monótono emerge. Esta pesquisa enfatiza o papel vital das correlações na supercondutividade robusta, oferecendo oportunidades de design de materiais sob medida.

Palavras-chave: desordem correlacionada; supercondutividade; amostras quase 1D; intensidade da desordem; correlações espaciais.

LIST OF FIGURES

Figure 1 – Graphic of resistence versus temperature obtained experimentally by Ommes for mercury. 12

Figure 2 – Left: Specific Heat versus temperature. Right: Helmholtz Energy versus temperature. 14

Figure 3 – Vacuum-Superconductor interface in presence of magnetic field. 17

Figure 4 – Representation of Meissner Effect. 18

Figure 5 – the representation of a Fermi sphere with an electron-Hole pair excitation on a non interacting gas. 19

Figure 6 – Vortices in a 200-nm-thick YBCO film 21

Figure 7 – Two crystalline lattices are represented. They are an example of what disorder means in our context: Displacements of atoms from their equilibrium position. Left: Representation of a ordered crystalline lattice. Right: Representation of a disordered crystalline lattice. 51

Figure 8 – Histogram of order parameter for several disorder values 55

Figure 9 – Histogram of local electron density for several disorder values. 56

Figure 10 – Appearance of superconducting islands with increasing disorder. The figure shows four different samples with the disorder strength (V) varying from t to 3t. The darker areas are the regions where the order parameter is non-zero, while white areas are where order parameters are zero. 56

Figure 11 – Appearance of superconduting islands in superconducing sample with increasing disorder and correlation in the random potential. Row (a) shows the evolution of the disorder potential as the correlation increases. Rows (b) - (e) shows the local order parameter evolves with increasing disorder and correlation degree. The white areas is where the order parameter is zero whereas blue areas indicate non-zero order parameter. In this figure since t $= 1$, the disorder strength V has only numerical values, but of course we can multiply the number for t and the disorder strength would be the same. 60

Figure 12 – Figures (a) - (c) Histogram of order Parameter for different potentials and correlations. The histogram is normalized in relation to the average order parameter $\overline{\Delta}$. 61

Figure 13 – Average order parameter $\overline{\Delta}$ versus width (or confinement length) without disorder. 65
Figure 14 – Average order parameter $\overline{\Delta}$ versus width for $\alpha = 0$. 67
Figure 15 – Average order parameter $\overline{\Delta}$ versus width for V = 0.1t. 67
Figure 16 – Average order parameter $\overline{\Delta}$ versus width for V = 0.3t. 68
Figure 17 – Average order parameter $\overline{\Delta}$ versus width for V = 0.5t. 68
Figure 18 – Average order parameter $\overline{\Delta}$ versus width for V = 0.75t. 69
Figure 19 – Average order parameter $\overline{\Delta}$ versus width for V = 1.0t. 69
Figure 20 – Histogram of Order Parameter for sample with size: 5x64. 70
Figure 21 – Histogram of Order Parameter for sample with size: 6x64. 70
Figure 22 – Histogram of Order Parameter for sample with size: 7x64. 70
Figure 23 – Histogram of Order Parameter for sample with size: 8x64. 71
Figure 24 – Histogram of Order Parameter for sample with size: 9x64. 71
Figure 25 – Histogram of Order Parameter for sample with size: 5x64. 71
Figure 26 – Histogram of Order Parameter for sample with size: 6x64. 72
Figure 27 – Histogram of Order Parameter for sample with size: 7x64. 72
Figure 28 – Histogram of Order Parameter for sample with size: 8x64. 72
Figure 29 – Histogram of Order Parameter for sample with size: 9x64. 73
Figure 30 – Histogram of Order Parameter for sample with size 32x64 for V = 0.1t. . . 74
Figure 31 – Histogram of Order Parameter for sample with size 32x64 for V = 0.3t. . . 74
Figure 32 – Histogram of Order Parameter for sample with size 32x64 for V = 0.5t. . . 75
Figure 33 – Histogram of Order Parameter for sample with size 32x64 for V = 0.75t. . 75
Figure 34 – Histogram of Order Parameter for sample with size 32x64 for V = 1.0t. . . 76

CONTENTS

1 INTRODUCTION TO SUPERCONDUCTIVITY 12

1.1 THE DISCOVERY OF SUPERCONDUCTIVITY 12

1.2 THERMODYNAMIC QUANTITIES 13

1.3 PERFECT DIAMAGNETISM: THE LONDON EQUATION 14

1.4 MEISSNER EFFECT 16

1.5 ABSENCE OF LOW ENERGY EXCITATIONS 18

1.6 TWO KINDS OF SUPERCONDUCTIVITY 20

2 BCS THEORY 22

2.1 COOPER PAIR 22

2.2 ORIGIN OF THE ATTRACTIVE INTERACTION 25

2.3 BCS GROUND STATE 27

2.4 VARIATIONAL METHOD 29

2.5 APPROACH VIA CANONICAL TRANSFORMATIONQ 32

2.6 FINITE TEMPERATURE 36

3 THE BOGOLIUBOV DE GENNES EQUATION 39

3.1 INTRODUCTION 39

3.2 HUBBARD MODEL 40

3.3 DERIVATION OF BDG EQUATIONS 41

3.4 CHEBYSHEV BDG METHOD 46

3.4.1 The Hamiltonian 46

3.4.2 BdG Equation 47

3.4.3 Spectral Density 47

3.4.4 Orthogonal Polynomials 48

4 DISORDER IN SUPERCONDUCTORS 51

4.1 ANDERSON THEOREM FOR DISORDERED SUPERCONDUCTORS . . . 52

4.2 STRONG DISORDER EFFECTS 54

4.3 CORRELATED DISORDER 57

4.4 EFFECTS OF CORRELATED DISORDER ON SUPERCONDUCTIVITY . . 59

5 RESULTS AND DISCUSSION 62

5.1 QUANTUM OSCILATIONS IN THE ORDER PARAMETER 62

5.2 CASE WITH NON-CORRELATED DISORDER 66
5.3 CASE WITH CORRELATED DISORDER 67
6 CONCLUSION 77
REFERENCES 79

1 INTRODUCTION TO SUPERCONDUCTIVITY

1.1 THE DISCOVERY OF SUPERCONDUCTIVITY

Superconductivity is a centenary research field. It was begun in Laiden – Netherlands, 8th of April, 1911. Heike Kamerling Onnes, at his laboratory, observed for the first time the phenomena of superconductivity, that is, the abrupt disappearance of electric resistance in metals bellow a certain critical temperature (T_c). There were two main theories about what would happen to resistance when the temperature approached zero: 1 - It was believed that resistance would approach zero as the temperature goes to zero as well, never being zero before that. 2 – It was also believed that resistance would be infinity, based on the freezing of electrons on the material. The critical temperature is, at that time, very low. The highest critical temperature was about 23 K until 1983. Such kind of experiment and detection was only possible because few years before, Onnes had managed to turn Helium into a liquid (also for the first time). Mercury was one of the metals used for experiments since it is easy to find it in a high purity degree. All others materials used in the experiment has some residual resistance, which Onnes believed to be due to the presence of impurities (COSTA; PAVãO, 2012). The abrupt fall of electrical resistance at 4,2 K intrigued Onnes. Due to his investigations on material at very low temperatures, which lead to the production of liquid helium, Onnes was awarded the Nobel Prize in 1913 (IEEE, 2022).

Figure 1 – Graphic of resistence versus temperature obtained experimentally by Ommes for mercury.

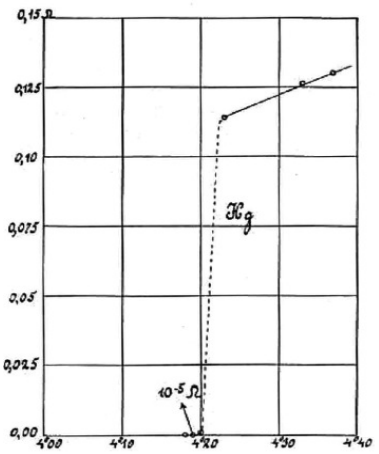

Source: Vernède (2011)

Later, in 1933, Walther Meissner and Robert Ochsenfeld verified that superconducting

materials are able to expell totally the magnetic field from inside its interior (perfect diamagnetism). This effect is known nowadays as Meissner Effect. Actually, the magnetic field can penetrate the material in a characteristic length called London penetration length, which varies from material to material. There is one (or more) critical field in a superconductor, for strong enough magnetic field the superconductivity (superconducting state) is destroyed and the material becomes normal again (normal state). No explanation was given at that time, but it was clear that no theory for conductors could be assigned to explain such effect. It was only in 1935 when London Brothers came up with an explanation. Then, the superconducting is interpreted as a new state of matter, the superconducting state. The critical temperature that divide the superconducting and normal state is characterized by a phase transition, where it is present discontinuities on thermodynamics parameters such as specific heat. Although several very successful theories were developed to explain superconductivity, the explanation of high temperature superconductors (that is, the critical temperature is comparable with environment temperatures) remains side by side with Fractionary Quantum Hall Effect as one of the most mysterious phenomena in condensed matter physics. The High Temperature Superconductors are being discovered as time passes. In 2021, the superconductor with the highest critical temperature at ambient pressure is the cuprate of mercury, barium and calcium at around 133K. There are other superconductors with higher transition temperatures, but these only occur at very high pressures (SCHILLING et al., 1993) (DROZDOV et al., 2019). It is not completely known for exotic superconductors how the mechanism behind superconducting electrons actually works. Besides, theories as Ginzburg Landau (GL), Barder Cooper and Schrieffer (BCS) gave us a lot of knowledge about how conventional superconductivity happens. So far, 11 physicists were awarded with Nobel prizes for who their efforts to superconductivity, among them, legendary names as Lev Landau, Alexei Abrikosov, Leon Cooper and Heike Onnes himself are valid to mention. The applications for superconductors are straightforward. No resistance means non dissipative current, the possibility of transport electric current through several kilometers without losing energy may become possible in a few decades. Moreover, applications of quantum computer devices and magnetic levitation are promising as well.

1.2 THERMODYNAMIC QUANTITIES

As said in the previous section, the superconductivity, a new condensate state, is characterized by a phase transition, which can be measured via thermodynamics quantities like

Helmholtz energy and specific heat. The Helmholtz energy can be derived from the specific heat data and it is shown in the figure 2.

Figure 2 – Left: Specific Heat versus temperature. Right: Helmholtz Energy versus temperature.

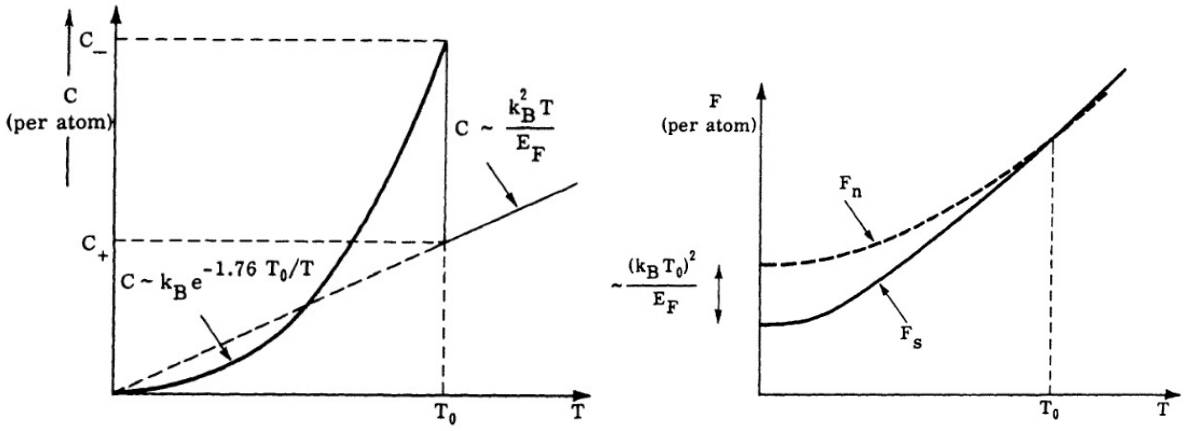

Source: Gennes (1999)

We see in Figure 2 (a) the behavior of the specific heat. At the critical temperature, here labelled T_0, there is a discontinuity, which characterizes the phase transition between normal and superconducting state. The behavior close to temperature zero resembles (and actually is) an exponential. The reader who remembers statistical mechanics can be confidant to affirm that this characterizes the existence of a gap between the ground state and the excitation levels. In Figure 1.2 (b), the Helmholtz Energy is shown for a normal metal and superconducting state, F_n (dashed line) and F_s (continuous line), respectively. From the critical temperature and bellow, these lines split, the actual state is the superconducting state since it is less energetic. As the temperature approaches zero, the difference between energies, $(F_s - F_n)|_{T=0}$ is called condensation energy. The symbols E_F and k_B mean respectively Fermi Energy and Boltzmann constant.

1.3 PERFECT DIAMAGNETISM: THE LONDON EQUATION

If we now want to have a description about how magnetic field interact with superconductors, we can rely on an energetic analysis. Here, let us consider that $j_s(\mathbf{r})$ indicates supercurrents, that is, the electric current whose charge caries in movement are superconducting electrons, and the associated magnetic field $\mathbf{h}(\mathbf{r})$ in the sample. Let us also consider the limit where all currents and fields are weak and the spatial variations are slow.

As usual, we know that in a metal we can approximate the bottom of a electronic band

using a parabolic relation. Considering electrons with effective mass m, the free energy has the following form:

$$\mathcal{F} = \int F_S d\mathbf{r} + E_{kin} + E_{mag}, \tag{1.1}$$

E_{kin} is the kinetic energy associated with the superconducting currents, E_{mag} is the magnetic energy, and F_S is the energy of the electrons in the condensate state at rest.

Consider that the drift velocity of electrons at a point $\mathbf{r}$ is $\mathbf{v}(\mathbf{r})$. The relation with the superconducting current is

$$n_S e\mathbf{v}(\mathbf{r}) = j_S(\mathbf{r}) \tag{1.2}$$

, where e is the electron charge, and n_s is the density of superconducting electrons. We have then

$$E_{kin} = \int d\mathbf{r} \frac{1}{2} m v^2 n_S \tag{1.3}$$

with the integral covering all superconducting material. The expression above is nothing but the integral of all kinetic energy in the material. Since we are in the limit of very slow spatial variations, the expression inside the integral is approximately constant.

At last, the magnetic energy E_{mag} is given by:

$$E_{mag} = \int \frac{h^2}{8\pi} d\mathbf{r}. \tag{1.4}$$

The field is related to j_S using the Ampere's Law:

$$\nabla \times \mathbf{h} = \frac{4\pi}{c} j_S. \tag{1.5}$$

Mixing all equations above by writing everything in terms of magnetic fields, we obtain the following expression for the free energy:

$$\mathcal{F} = \int F_S d\mathbf{r} + \frac{1}{8\pi} \int [\mathbf{h}^2 + \lambda_L^2 |\nabla \times \mathbf{h}|^2] d\mathbf{r}, \tag{1.6}$$

where λ_L is

$$\lambda_L = \left[\frac{mc^2}{4\pi n_S e^2} \right]^{1/2}. \tag{1.7}$$

Since n_S is the density of superconducting electrons, as we approach T=0, n_S approachs n, the total density of electrons.

As any usual problem of obtaining an equation of motion from an functional energy, we shall employ the use of variational calculus to find the equation that rules h. Let us change $\mathbf{h}(\mathbf{r})$ by $\delta\mathbf{h}(\mathbf{r})$, making $\mathcal{F}$ changes by $\delta\mathcal{F}$ in the same way:

$$\delta\mathcal{F} = \frac{1}{4\pi} \int [\mathbf{h} \cdot \delta\mathbf{h} + \lambda_L^2 (\nabla \times \mathbf{h}) \times \nabla\delta\mathbf{h}] d\mathbf{h}, \tag{1.8}$$

by using integral by parts in the last term on the right hand side, assuming that changes in the border of the superconducting material vanishes, we have

$$\delta\mathcal{F} = \frac{1}{4\pi}\int[\mathbf{h} + \lambda_L^2\nabla\times(\nabla\times\mathbf{h})]\cdot\delta\mathbf{h}d\mathbf{r}. \tag{1.9}$$

The field which minimizes the energy is obtained by $\delta\mathcal{F}$ to zero, being valid for any shape, the integrand must be zero:

$$\mathbf{h} + \lambda_L^2\nabla\times(\nabla\times\mathbf{h}) = 0. \tag{1.10}$$

The equation above is the celebrated London Equation. It is able to explain, as we shall see, the Meissner Effect. Combined with Ampere's law it is possible to obtain the suppression of superconducting currents in presence of external magnetic fields as well.

1.4 MEISSNER EFFECT

The London Equation gives us some details about what happens when a magnetic field penetrates the superconductor. Let us try to solve it for a simple superconductor with easy-to-work symmetry. Let us assume that the interface of the superconductor lies in the xy plane. For z $<$ 0 the space is empty. The field and current only depends on z. In addition to equation (1.10), we can use also Ampere's and Gauss' law for magnetism:

$$\nabla\times\mathbf{h} = \frac{4\pi j_s}{c} \tag{1.11}$$

$$\nabla\cdot\mathbf{h} = 0. \tag{1.12}$$

The possibility of **h** being parallel to z is ruled out since from gauss law, $\partial h/\partial z = 0$, **h** is constant in space. Then, $\nabla\times\mathbf{h} = 0$, implying that **h** and j_s are zero.

The second possibility is h is parallel to the interface, let us say, x axis. Gauss' law for magnetism is automatically satisfied since their derivatives only affects the same component. The Ampere's law have non zero result:

$$\frac{dh}{dz} = \frac{4\pi j_s}{c}. \tag{1.13}$$

Using the London Equation and the Ampere's law we obtain:

$$\frac{dj_s}{dz} = \frac{4\pi\lambda_L^2}{c}h, \tag{1.14}$$

Figure 3 – Vacuum-Superconductor interface in presence of magnetic field.

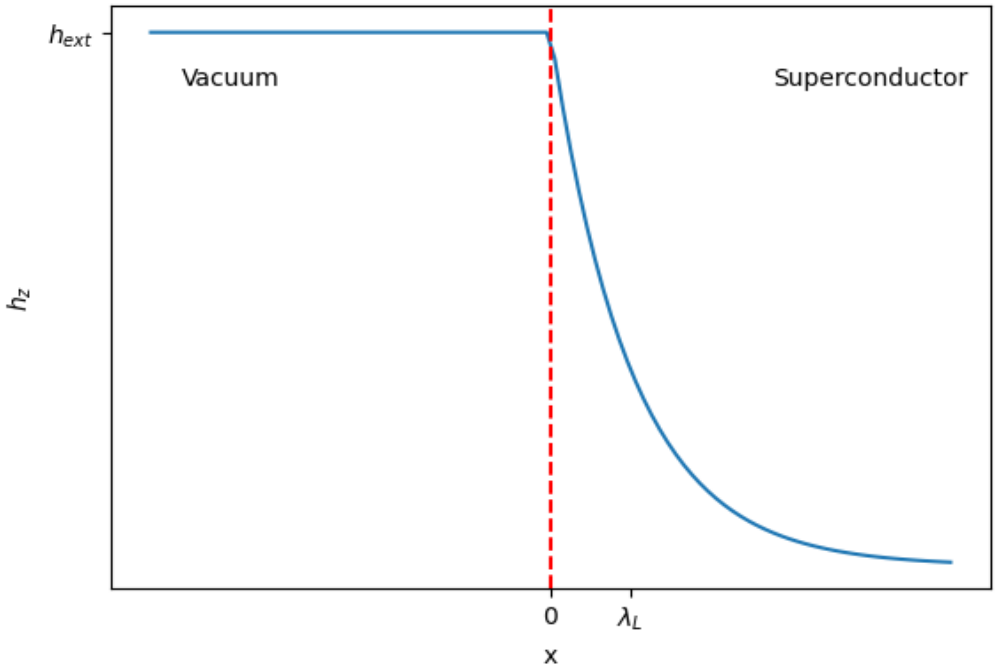

Source: The author (2023).

$$\frac{d^2h}{dz^2} = \frac{h}{\lambda_L^2}. \tag{1.15}$$

The solutions decreases exponentially as the field gets deeper inside the superconductor,

$$h(z) = h(0)\exp(-z/\lambda_L). \tag{1.16}$$

It is possible to see here that the magnetic field can indeed penetrate some depth inside the superconductor. This depth is measured in terms of the penetration length λ_L. In fact, it is possible to generalize to any sample, a weak enough magnetic field is practically expelled from the sample apart from a surface. The superconductor finds an equilibrium state where the sum of kinetic and magnetic energies is minimum, and this state, for macroscopic samples, corresponds to the expulsion of magnetic flux.

For strong enough magnetic fields it is possible to destroy partially or totally the superconducting state, producing magnetic vortices or turn the sample into a normal metal again.

Figure 4 – Representation of Meissner Effect.

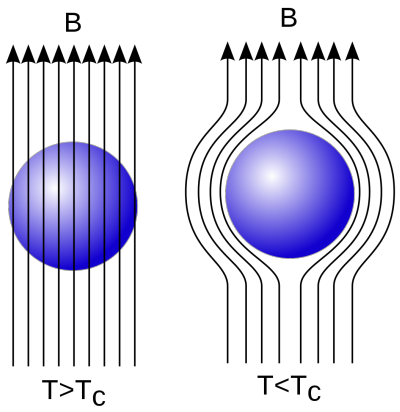

Source: Wikimedia Commons (2005)

1.5 ABSENCE OF LOW ENERGY EXCITATIONS

The ground state of an non interacting electron gas can be described by putting every electron on the lowest state possible. Once one electron occupies the actual lower state of the system, the next electron will occupy the next lowest state, one energy level above from the previous electron (if the system is not degenerated and not considering spin). After filling all lower energy states with all electrons in the system, it is formed a sphere in the momentum space with radius p_F, the momentum of the most energetic electron in the system, such sphere is called Fermi Sphere. The most energetic electron has the energy E_F, the Fermi energy. Above such energy, all levels are empty. If we want to build an excitation in such system, we only have to provide energy to extract one electron with momentum $p < p_F$ to a level with momentum (and energy) greater than p_F. Allowing one energy level empty in such sphere leads us to the concept of holes: the lack of electrons in a filled electron sphere in momentum space behaves like an electron with positive charge. Thus, excitation of the system from the ground state by adding some energy leads to the formation of an electron-hole pair, which is called electron-hole excitation. For such an excitation, which satisfies the previous assumptions, the following energy costs are required:

$$E_{pp'} = \frac{p'^2 - p^2}{2m} \geq 0. \tag{1.17}$$

If the number of electrons is large, this excitation can be arbitrarily small, since both momenta p' and p are close to the Fermi momentum. In a metal, the discussion is quite similar, the Fermi sphere can be modified, leading to non-spherical shapes, but the excitations are still

very small. From solid state physics, we know that:

- The specific heat is relatively large and proportional to T. (see (KITTEL, 2004))
- Strong dissipate effects take place when electrons are submitted to low frequency external peturbations, such as electromagnetic waves. (see (BRUUS; FLENSBERG, 2004))

Figure 5 – the representation of a Fermi sphere with an electron-Hole pair excitation on a non interacting gas.

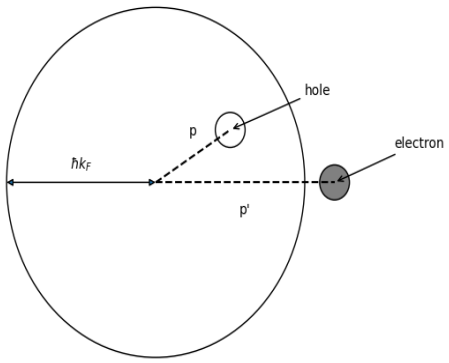

The Author (2023).

In most superconductors, the energy $E_{p'p}$ necessary to create a electron-hole pair is

$$E_{p'p} \geq 2\Delta. \tag{1.18}$$

Roughly speaking, Δ is the "gap", also called "paring energy" and it is related to the critical temperature, $2\Delta \approx 3.5 k_B T_c$ (GENNES, 1999). Notice that 2Δ is the energy to create a pair excitation. The energy per excitation is Δ.

There are several methods for detecting the gap:

- The low temperature specific heat is now proportional to $\exp(-\Delta/k_B T)$. It is quite analogous to the deviation from Einstein's solid specific heat and an actual solid specific heat. The existence of a gap between the ground state and the first excited state gives this exponential behavior.

- Absortion of electromagnetic energy. For photons with $\hbar\omega \geq 2\Delta$ it is possible to create a electron-hole pair. The typical wave length are in the 1mm range.

- Ultrasonic attenuation. A phonon of low frequency cannot decay into a electron-hole pair excitation, but it can be absorbed by collisions by others preexisting excitations. This process is proportional to the number of preexisting excitations, thus $\exp(-\Delta/k_B T)$.

One important information is that the existence of a gap is not a necessary condition for the existence of superconductivity. It is possible using other mechanisms to obtain gapless excitations. One example is the excitations on surface superconductivity. This topic is beyond the scope of this dissertation, but a good reference is given at de Gennes (GENNES, 1999).

1.6 TWO KINDS OF SUPERCONDUCTIVITY

We have assumed previously on derivation of London equation that $v(\mathbf{r})$ varies slowly. In the condensate state, the velocity of two electrons are correlated if the distance between them are smaller than a certain range. For pure superconductors, the correlation length is called ξ_0. The derivation of London equation applies when $v(\mathbf{r})$ has negligible variations over distances ξ_0. To estimate ξ_0 we notice that the important domain in momentum space is defined by

$$E_F - \Delta < \frac{p^2}{2m} < E_F + \Delta. \tag{1.19}$$

The thickness of the shell in p space defined by the equation above if $\delta p \approx 2\Delta/v_F$, where v_F is the Fermi velocity, defined by $v_F \equiv p_F/m$. We have assumed above that $\Delta \ll E_F$. A wave packet formed of plane waves whose momentum has an uncertainty δp has a minimum spatial extent $\delta x \sim \hbar/\delta p$. This leads we to

$$\xi_0 = \frac{\hbar v_F}{\pi\Delta}, \tag{1.20}$$

the factor π on denominator appears for convenience. The length ξ_0 is called coherence length of the superconductor.

Now we have two different lengths on a superconductor, ξ_0 and λ_L. By defining the quantity $\kappa = \lambda_L/\xi_0$, we can separate two kinds of superconductors:

- $\kappa < 1/\sqrt{2}$, type I superconductors. Presents only one critical magnetic field which completely destroys superconductivity. In non-transition metals, λ_L is small (~ 300Å). The Fermi velocity is large ($v_F \sim 10^8 cm/s$) and ξ_0 is large ($\sim 10^4$Å for aluminum). Our

assumption on London Equation derivation relied on $\lambda_L \gg \xi_0$ (show spatial variation). Thus London equation does not apply to such situation.

- $\kappa > 1/\sqrt{2}$, type II superconductors. Presents two critical magnetic fields. The lower critical field destroys the superconductivity at certain well defined regions, generating around such regions current vortices. These vortices are called Abrikosov Vortices. The upper critical field completely destroys superconductivity. For transition and intermetalic compounds, the effective mass is very large, λ_L is large (~ 2000Å) and Fermi velocity is small ($\sim 10^6 cm/s$). It is found that in such compounds the critical temperature is high (18^oK in Nb_3Sn). We will see later that Δ is proportional to the critical temperature T_c. For all these reasons, ξ_0 is very small (~ 50Å). The London equation works well for this class of material.

Figure 6 – Vortices in a 200-nm-thick YBCO film

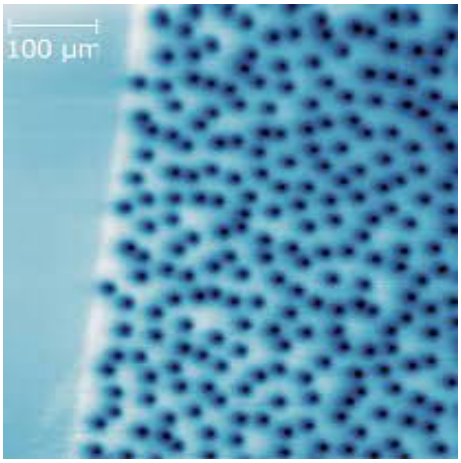

Source: Wikimedia Commons (2015)

2 BCS THEORY

The theory of superconductivity from microscopic principles was showed for the first time for J. Bardeen, L. N. cooper, and J. R Schrieffer, the so-called BCS Theory (BARDEEN; COOPER; SCHRIEFFER, 1957). Few years before, L. Landau and V. Ginzburg proposed a phenomenological theory to describe superconductivity close to the critical temperature. That did not received much attention. Years later, L. Gor'kov showed that the phenomenological theory could be derived from BCS Theory. It is impressive that L. Landau and V. Ginzburg managed to derive from much of intuition. This dissertation is not going to focus on phenomenological theory. Instead, the BCS Theory here is introduced to give space to the Bogoliubov-de Gennes equation, which will be derived next section.

2.1 COOPER PAIR

A bound state between two electrons seems to be a very weird idea at first glance. In fact, the origin of the attractive interaction will be discussed later, but it is important here to how to existence of such state regardless how small the attractive interaction is. Such effect is possible because the Fermi sea (all electrons in the lowest energy level possible) unstable against the formation of at least one bound pair. Such effect is consequence of two effects: the Fermi statistics and the existence of a Fermi-sea in the background. Bound states usually does not occur in two-body problem in three dimensions until the strength of the potential exceeds a finite threshold value.

Let us say that two electrons are added to the Fermi sea at temperature equal zero (T = 0). The electrons can interact with each other via an attractive interaction only - they cannot interact with the electrons in the Fermi sea unless via exclusion principle (that is, they cannot occupy levels bellow the Fermi energy). The hamiltonian of this problem can be written as

$$\left[-\frac{\hbar^2\nabla^2_{\mathbf{r}_1}}{2m} - \frac{\hbar^2\nabla^2_{\mathbf{r}_2}}{2m} + V(\mathbf{r}_1 - \mathbf{r}_2)\right]\Psi(\mathbf{r}_1, \mathbf{r}_2) = E\Psi(\mathbf{r}_1, \mathbf{r}_2), \tag{2.1}$$

where $\Psi(\mathbf{r}_1, \mathbf{r}_2)$ is the wave-function for two electrons and E is the energy. Since it is a two body problem, it is possible to change for center of mass coordinates $\mathbf{r} = \frac{1}{2}(\mathbf{r}_1 + \mathbf{r}_2)$ and the relative coordinates $\mathbf{r} = \frac{1}{2}(\mathbf{r}_1 - \mathbf{r}_2)$. It is straightforward to show that

$$\left[-\frac{\hbar^2\nabla^2_{\mathbf{r}}}{2m^*} - \frac{\hbar^2\nabla^2_{\mathbf{r}}}{2\mu} + V(\mathbf{r})\right]\Psi(\mathbf{r}, \mathbf{r}) = E\Psi(\mathbf{r}, \mathbf{r}). \tag{2.2}$$

Here, $m^* = 2m$ and $\mu = m/2$, the reduced mass. The seek for a two-particle wavefunction. By general arguments of Bloch, we expect that the wavefunction can be separated into a part that depends on **r** and other that depends on **r**.

$$\Psi(\mathbf{r}, \mathbf{r}) = \psi(\mathbf{r}) \exp(i\mathbf{k} \cdot \mathbf{R}). \tag{2.3}$$

The vector **k** give us the wave vector due to the movement of the center of mass. This will give us a new Schrodinger equation with a rescaled energy

$$\left[-\frac{\hbar^2 \nabla^2}{2\mu} + V(\mathbf{r})\right] \psi(\mathbf{r}) = \tilde{E}\psi(\mathbf{r}), \tag{2.4}$$

where $\tilde{E} = E - \frac{\hbar^2 K^2}{2m'}$. For a given E, the lowest $\tilde{E}$ is the one for which $\mathbf{k} = 0$, that is, when the momentum of center of mass vanishes. Making $\mathbf{k} = 0$ makes the particle having opposite momentum, let us work with this assumption from now on. Depending on the symmetry of the spatial part we can have a singlet or triplet state for the spin. Anticipating an attractive interaction, we choose an symmetric spatial part since the lowest energy happens when electrons are close to each other. This implies on a singlet spin state, which leads us to build the following wave function:

$$\psi(\mathbf{r}) = \left[\sum_{\mathbf{k}>\mathbf{k}_F} g_{\mathbf{k}} \cos(\mathbf{k} \cdot \mathbf{r})\right] (\alpha_1\beta_2 - \beta_1\alpha_2), \tag{2.5}$$

where α_i and β_i are spin variables for particle 1 and 2, the interacting electrons. They are build in such way to produce a antissymetric state for the spin so that the total wavefunction is antissymetric, leading us to a fermionic behavior, as it should be. Let us insert our wavefunction into the Schrodinger equation, working on the derivatives and reminding that $\tilde{E} = E$ produces (suppressing spin variables)

$$\sum_{\mathbf{k}>\mathbf{k}_F} [2\epsilon_{\mathbf{k}} + V(\mathbf{r})] g_{\mathbf{k}} \cos(\mathbf{k} \cdot \mathbf{r}) = E \sum_{\mathbf{k}>\mathbf{k}_F} g_{\mathbf{k}} \cos(\mathbf{k} \cdot \mathbf{r}), \tag{2.6}$$

where $\epsilon_{\mathbf{k}}$ is the non-perturbed plane-wave energies, $\frac{\hbar^2 k^2}{2m}$. Using the fact that $V(\mathbf{r})$ is an even function and performing Fourier transformation in all equation we obtain

$$(E - 2\epsilon_{\mathbf{k}}) g_{\mathbf{k}} = \sum_{\mathbf{k}'>\mathbf{k}_F} V_{\mathbf{k}\mathbf{k}'} g_{\mathbf{k}'}. \tag{2.7}$$

where

$$V_{\mathbf{k}\mathbf{k}'} = \Omega^{-1} \int V(\mathbf{r}) e^{i(\mathbf{k}'-\mathbf{k})\cdot\mathbf{r}} d\mathbf{r}, \tag{2.8}$$

Ω being the normalization volume. $V_{\mathbf{k}\mathbf{k}'}$ connects scattering between electrons with momentum $(\mathbf{k}', -\mathbf{k}')$ to $(\mathbf{k}, -\mathbf{k})$. If we can find a set of $g_{\mathbf{k}}$ that satisfies the equation above, with $E < 2E_F$, then a bound-pair state exist.

It is quite hard to analyse the equation for $g_{\mathbf{k}}$ with such general potential. Cooper introduced an approximation

$$V_{\mathbf{k}\mathbf{k}'} = \begin{cases} -V & \text{if } \epsilon_{\mathbf{k}}, \epsilon_{\mathbf{k}'} < \omega_c \hbar, \\ 0 & \text{otherwise.} \end{cases} \tag{2.9}$$

It is constant inside a certain cutoff energy, and zero outside. The right-hand of equation 2.6 becomes then

$$g_{\mathbf{k}} = V \frac{\sum g_{\mathbf{k}'}}{2\epsilon_{\mathbf{k}} - E}. \tag{2.10}$$

Summing both sides and canceling $\sum g_{\mathbf{k}}$, we obtain

$$\frac{1}{V} = \sum_{\mathbf{k} > \mathbf{k}_F} (2\epsilon_{\mathbf{k}} - E)^{-1}. \tag{2.11}$$

In the continuum limit, we can change the summation for an integral on energy levels by adding the density of states. The density of states can be set at the Fermi level since the cutoff is much smaller than the Fermi level:

$$\frac{1}{V} = N(0) \int_{E_F}^{E_F + \hbar\omega_c} \frac{d\epsilon}{2\epsilon - E} = \frac{1}{2} N(0) \ln \left(\frac{2E_F - E + 2\hbar\omega_c}{2E_F - E} \right), \tag{2.12}$$

N(0) indicating the density of states at the Fermi level. In case of the weak-coupling case, there $N(0)V \ll 1$, few approximations produce

$$E \approx 2E_F - 2\hbar\omega_c e^{-2/N(0)V} \tag{2.13}$$

Since the energy is smaller than twice the Fermi level, we see that it is possible to have a bound state with negative energy with respect to the Fermi surface made up entirely of electrons with $\mathbf{k} > \mathbf{k}_F$, that is, with kinetic energy in excess of E_F. The contribution to the energy of the attractive potential outweighs this excess of kinetic energy, leading to a binding regardless of how small V is. It is important to notice that the binding energy depends on the inverse of V, that is, not analytic at V = 0 - it cannot be expanded in powers of V, thus it cannot be derived using perturbation theory. This fact delayed the genesis of the theory.

After all calculations so far, the wavefuntion $\psi(\mathbf{r})$ is proportional to

$$\sum_{\mathbf{k} > \mathbf{k}_F} \frac{\cos(\mathbf{k} \cdot \mathbf{r})}{2\xi_{\mathbf{k}} + E'}, \tag{2.14}$$

where here we have changed energies from the Fermi energy

$$\xi_{\mathbf{k}} = \epsilon_{\mathbf{k}} - E_F \quad \text{and} \quad E' = 2E_F - E > 0. \tag{2.15}$$

Now we see that due to the change of sing, E' is the binding energy with respect to $2E_F$. Since $g_{\mathbf{k}}$ depends only on $\xi_{\mathbf{k}}$, the solution has spherical symmetry, we call it s-wave superconductor. It is quite important in this dissertation because all superconducting effects developed on final results here will be on s-wave superconductors. Also, the weighting factor $(2\xi_{\mathbf{k}} + E')^{-1}$ has its maximum at value $1/E'$ when $\xi_{\mathbf{k}} = 0$. Electron states within a range of energy E' above E_F are those most strongly involved in forming the bound state. Since $E' \ll \hbar\omega_c$ for $N(0)V \ll 1$, this shows that the detailed behavior of $V_{\mathbf{kk}'}$ our around $\hbar\omega_c$ will not have any great effect on the result. That is why I have performed such rough approximation before.

Returning to the total energy, we can write then the binding plus kinetic energy as

$$E = \tilde{E} + \frac{\hbar^2 K^2}{4m} = 2\epsilon_{\mathbf{k}} - E' + \frac{\hbar^2 K^2}{4m}. \tag{2.16}$$

In the limit that $E \to 2\epsilon_{\mathbf{k}}$, we can still obtain a bound state with finite center of mass momentum:

$$K = \frac{2}{\hbar}\sqrt{mE'}. \tag{2.17}$$

This gives rise to a finite current density

$$J = n_s e\frac{\hbar K}{m} = 2n_s e\sqrt{\frac{E'}{m}}. \tag{2.18}$$

2.2 ORIGIN OF THE ATTRACTIVE INTERACTION

As discussed previously, a simple electron gas cannot form bound states. To achieve attractive behavior in the potential $V_{\mathbf{kk}'}$, it is necessary to couple the system to other particles or excitations. In solids, various elementary excitations exist, such as phonons, electrons from other bands, spin waves, and polarons. In our present scenario, the electron-phonon interaction plays a significant role. Although there are other types of interactions that can lead to bound states, they are beyond the scope of this dissertation.

The matrix element $V_{\mathbf{kk}'}$ of electron-electron interaction connects states with different momentum, obeying conservation laws. Generally, $V_{\mathbf{kk}'}$ can be expressed in two terms:

- The direct Coulomb repulsion U_c connects two electrons (from state I to II):

$$\langle I|H_c|II\rangle = \int d\mathbf{r}_1 d\mathbf{r}_2 e^{-i\mathbf{k}\cdot(\mathbf{r}_1-\mathbf{r}_2)} U_c(\mathbf{r}_1-\mathbf{r}_2) e^{i\mathbf{k}'(\mathbf{r}_1-\mathbf{r}_2)} \tag{2.19}$$

$$= \int U_c(\rho) d\rho e^{i\mathbf{q}\cdot\rho} = U_{\mathbf{q}}. \quad \mathbf{q} = \mathbf{k}' - \mathbf{k}. \tag{2.20}$$

- One electron may emit a phonon, which can be later absorbed by another electron. The initial state has energy

$$E_I = 2\xi_{\mathbf{k}}, \tag{2.21}$$

as defined in Equation 2.15, and the final state has energy

$$E_{II} = 2\xi_{\mathbf{k}'}, \tag{2.22}$$

Momentum conservation allows for two intermediate states:

  - Electron 1 in state $\mathbf{k}' = \mathbf{k} + \mathbf{q}$, and electron 2 in $-\mathbf{k}$, where a phonon is created with wave vector $-\mathbf{q}$ and energy $\hbar\omega_q$

$$E_{i2} = \xi_{\mathbf{k}'} + \xi_{\mathbf{k}} + \hbar\omega_q = E_{i1}. \tag{2.23}$$

    Here, $\xi_{\mathbf{k}}$ and $\omega_{\mathbf{k}}$ are even functions.

  - Electron 1 in state $\mathbf{k}$, and electron 2 in $-\mathbf{k}' = -(\mathbf{q}+\mathbf{q})$, where a phonon is created with wave vector $\mathbf{q}$ and energy $\hbar\omega_q$

$$E_{i2} = \xi_{\mathbf{k}'} + \xi_{\mathbf{k}} + \hbar\omega_q = E_{i1}. \tag{2.24}$$

The second-order matrix element that couples states (I) and (II) due to electron-phonon (ep) interaction can be expressed as follows:

$$\langle I|H_{ep}|II\rangle = \sum_i \langle I|H_{ep}|i\rangle \frac{1}{2}\left(\frac{1}{E_{II}-E_i} + \frac{1}{E_I - E_i}\right)\langle i|H_{ep}|II\rangle. \tag{2.25}$$

The summation includes all allowed intermediate states. However, since we only have two allowed intermediate states, we can define W_q as follows:

$$\langle I|H_{ep}|II\rangle = \frac{|W_q|^2}{\hbar}\left(\frac{1}{\omega-\omega_q} - \frac{1}{\omega+\omega_q}\right). \tag{2.26}$$

Here, $\hbar\omega = \xi_{\mathbf{k}'} - \xi_{\mathbf{k}}$. The total matrix for the interaction is then given by:

$$\langle I|H|II\rangle = U_{\mathbf{q}} + \frac{2|W_q|^2}{\hbar}\frac{\omega_q}{\omega^2-\omega_q^2}. \tag{2.27}$$

When $\omega < \omega_q$, the indirect term can dominate the first term by introducing a negative component, resulting in an attractive potential, assuming U_q is not excessively large.

There are additional phenomena that need to be analyzed, such as the dielectric effect in solids. Interested readers are encouraged to refer to relevant literature (Kittel and de Gennes, to be cited later). However, the attractive interaction can be elucidated through the aforementioned electron-phonon interaction.

2.3 BCS GROUND STATE

We have seen that the Fermi sea is unstable against the formation of bound Cooper pairs when the total interaction among electrons is attractive. We expect that pairs will condense until an equilibrium is reached, characterized by a state of the system significantly different from the Fermi sea due to the large number of bound pairs. The binding energy for an additional pair becomes zero in this equilibrium state. To describe such a system with a large number of electrons, it is necessary to use second quantization (TINKHAM, 2004).

The Fermionic creation operator $\hat{c}^{\dagger}_{\mathbf{k}\sigma}$ creates an electron with momentum **k** and spin $\sigma = \uparrow, \downarrow$ (spin-up or spin-down). Similarly, the operator $c_{\mathbf{k}\sigma}$ destroys an electron. Using this notation, the singlet wavefunction can be written as

$$|\psi_0\rangle = \sum_{k>k_F} g_{\mathbf{k}} c^{\dagger}_{\mathbf{k}\uparrow} c^{\dagger}_{-\mathbf{k}\downarrow} |F\rangle, \tag{2.28}$$

where $|F\rangle$ represents the Fermi sea with all states filled up to k_F.

The BCS wavefunction can be approached by considering a general N-electron wavefunction expressed in terms of momentum eigenfunctions and incorporating Cooper pairing:

$$|\psi_N\rangle = \sum g(\mathbf{k}_i, ..., \mathbf{k}_l) c^{\dagger}_{\mathbf{k}_i\uparrow} c^{\dagger}_{-\mathbf{k}_i\downarrow} ... c^{\dagger}_{\mathbf{k}_l\uparrow} c^{\dagger}_{-\mathbf{k}_l\downarrow} |0\rangle, \tag{2.29}$$

where $|0\rangle$ represents the vacuum state (total absence of electrons), $\mathbf{k}_i$ and $\mathbf{k}_l$ designate the first and last of the M **k**-values in the band that are occupied in a given term in the sum, and g specifies the weight with which the product of this set of N/2 pairs of creation operators appears. Since there are

$$\frac{M!}{[M-(N/2)]!(N/2)!} \approx 10^{10^{20}} \tag{2.30}$$

ways of choosing N/2 states for pair occupancy, there will be a huge number of terms in the summation, making it impossible to determine. What BCS did is argue that due to the large

number of electrons in the system, it is sufficient to assume that electrons feel an average field created by all other electrons, known as the "mean field" of all occupied states. This is referred to as the Hartree self-consistent field. In its simplest form, this relaxes the constraint on the total number of particles being N, as occupancies are treated statistically. However, due to the large number of particles, in the thermodynamic limit, fluctuations in the number of particles are suppressed, and the average N, $\overline{N}$, is fixed when working with the grand canonical ensemble.

BCS considered the following wavefunction as their ground state:

$$|\psi_G\rangle = \prod_{\mathbf{k}=\mathbf{k}_1,\ldots,\mathbf{k}_M} (u_{\mathbf{k}} + v_{\mathbf{k}} c^\dagger_{\mathbf{k}\uparrow} c^\dagger_{-\mathbf{k}\downarrow})|0\rangle, \tag{2.31}$$

where $|u_{\mathbf{k}}|^2 + |v_{\mathbf{k}}|^2 = 1$. Here, the probability of finding a pair with $(\mathbf{k}\uparrow, -\mathbf{k}\downarrow)$ is $|v_{\mathbf{k}}|^2$, while the probability that it is unoccupied is $|u_{\mathbf{k}}|^2$. As mentioned before, the probabilities of finding N electrons in the system have a sharp peak at $\overline{N}$. This quantity can be calculated using

$$\langle\psi_G|N|\psi_G\rangle = \overline{N}, \tag{2.32}$$

where $N = \sum_{\mathbf{k},\sigma} c^\dagger_{\mathbf{k}\sigma} c_{\mathbf{k}\sigma}$. The calculation can be performed as follows:

$$\begin{aligned}
\overline{N} &= \left\langle \sum_{\mathbf{k},\sigma} c_{\mathbf{k}\sigma} c^\dagger_{\mathbf{k}\sigma} \right\rangle = \langle\psi_G| \sum_{\mathbf{k}} (c^\dagger_{\mathbf{k}\uparrow} c_{\mathbf{k}\downarrow} + c^\dagger_{\mathbf{k}\downarrow c_{\mathbf{k}}\downarrow})|\psi_G\rangle \\
&= 2\sum_{\mathbf{k}} \langle\psi_G| c^\dagger_{\mathbf{k}\uparrow} c_{\mathbf{k}\uparrow}|\psi_G\rangle \\
&= 2\sum_{\mathbf{k}} \langle 0|(u^*_{\mathbf{k}} + v^*_{\mathbf{k}} c_{-\mathbf{k}\downarrow} c_{\mathbf{k}\uparrow}) c^\dagger_{\mathbf{k}\uparrow} c_{\mathbf{k}\uparrow} (u_{\mathbf{k}} + v_{\mathbf{k}} c^\dagger_{\mathbf{k}\uparrow} c^\dagger_{-\mathbf{k}\downarrow}) \\
&\times \prod_{\mathbf{l}\neq\mathbf{k}} (u^*_{\mathbf{l}} + v^*_{\mathbf{l}} c_{-\mathbf{l}\downarrow} c_{\mathbf{l}\uparrow})(u_{\mathbf{l}} + v_{\mathbf{l}} c^\dagger_{\mathbf{l}\uparrow} c^\dagger_{-\mathbf{l}\downarrow})|0\rangle.
\end{aligned} \tag{2.33}$$

In the last equality, we have isolated operators from a single state to facilitate calculations. By separating the states, we can analyze the cases where $\mathbf{l} \neq \mathbf{k}$ and $\mathbf{l} = \mathbf{k}$. Since fermionic systems can have at most one electron per state, connecting states that preserve the same number of particles, we obtain

$$\overline{N} = \sum_{\mathbf{k}} 2|v_{\mathbf{k}}|^2. \tag{2.34}$$

Similarly, we can calculate the variation $\langle N^2\rangle - \overline{N}^2$ as similar to equation 2.33 and obtain

$$\langle N^2\rangle - \overline{N}^2 = 4\sum_{\mathbf{k}} u^2_{\mathbf{k}} v^2_{\mathbf{k}}. \tag{2.35}$$

Note that this is nonzero unless the occupancy cuts off discontinuously with $v_{\mathbf{k}}$ going from 1 to 0 and $u_{\mathbf{k}}$ from 0 to 1. Also, note that both $\overline{N}$ and $\langle(N - \overline{N})^2\rangle$ scale with the volume if we

compare systems of various sizes but the same particle density. Accordingly,

$$\delta N_{\text{rms}} = \langle (N - \overline{N})^2 \rangle^{1/2} \approx \overline{N}^{1/2} \approx 10^{10}, \tag{2.36}$$

while the fractional uncertainty is

$$\frac{\delta N_{\text{rms}}}{\overline{N}} \approx \frac{1}{\overline{N}^{1/2}} \approx 10^{-10}. \tag{2.37}$$

Thus, as is typical of many-particle statistical situations, as $N \to \infty$, the absolute fluctuations become large, but the fractional fluctuations approach zero.

2.4 VARIATIONAL METHOD

For a more broad understatement about the coefficients u and v, it is necessary to find explicit values for them. For that, let us define the pairing hamiltonian:

$$\mathcal{H} = \sum_{\mathbf{k}\sigma} \epsilon_{\mathbf{k}} n_{\mathbf{k}\sigma} + \sum_{\mathbf{kl}} c^{\dagger}_{\mathbf{k}\uparrow} c^{\dagger}_{-\mathbf{k}\downarrow} c_{-\mathbf{l}\downarrow} c_{\mathbf{l}\uparrow}, \tag{2.38}$$

where $n_{\mathbf{k}\sigma} = c^{\dagger}_{\mathbf{k}\sigma} c_{\mathbf{k}\sigma}$ counts the number of particles in the state with wavevector **k** and spin σ. The Hamiltonian in Equation 2.38 has all decisive terms for superconductivity, although it omits many other terms which involve electrons not paired. They may be important in other applications, but the idea is make it simple. To regulate the number of particles $\overline{N}$, we include a term $-\mu N$ (N here is the operator total average number of electrons $N = \sum_{\mathbf{k}\sigma} n_{\mathbf{k}\sigma}$), where μ is the chemical potential (or Fermi Energy for zero temperature). It is equivalent to taking the zero of the free electron energy to be μ. We ought to minimize the expectation value of the sum by setting

$$\delta \langle \psi_G | \mathcal{H} - \mu N | \psi_G \rangle = 0. \tag{2.39}$$

We know already from calculations very similar before that the free particle part can be calculated easily to produce

$$\langle \sum_{\mathbf{k}\sigma} \epsilon_{\mathbf{k}} n_{\mathbf{k}\sigma} - \mu N \rangle = 2 \sum \xi_{\mathbf{k}} |v_{\mathbf{k}}|^2 \tag{2.40}$$

where $\xi_{\mathbf{k}} = \epsilon_{\mathbf{k}} - \mu$.

Similarly, the interaction term gives

$$\langle V \rangle = \sum_{\mathbf{kl}} V_{\mathbf{kl}} u_{\mathbf{k}} v^*_{\mathbf{k}} u^*_{\mathbf{l}} v_{\mathbf{l}}. \tag{2.41}$$

Then all information above provides the following result:

$$\langle\psi_G|\mathcal{H}-\mu N|\psi_G\rangle = 2\sum \xi_{\mathbf{k}}|v_{\mathbf{k}}|^2 + \sum_{\mathbf{kl}} V_{\mathbf{kl}} u_{\mathbf{k}} v_{\mathbf{k}}^* u_{\mathbf{l}}^* v_{\mathbf{l}}, \tag{2.42}$$

which have to be minimized with the constraint $u_{\mathbf{k}}^2 + v_{\mathbf{k}}^2 = 1$. Since it reminds a very useful trigonometric relation, the constraint can be imposed by letting

$$u_{\mathbf{k}} = \sin\theta_{\mathbf{k}} \quad \text{and} \quad v_{\mathbf{k}} = \cos\theta_{\mathbf{k}}. \tag{2.43}$$

By substituting in the 2.42, and using few trigonometric properties as $\sin 2\theta = 2\sin\theta\cos\theta$ and $\sin^2\theta + \cos^2\theta = 1$, we obtain

$$\langle\psi_G|\mathcal{H}-\mu N|\psi_G\rangle = \sum_{\mathbf{k}} \xi_{\mathbf{k}}(1+\cos 2\theta_{\mathbf{k}}) + \frac{1}{4}\sum_{\mathbf{kl}} V_{\mathbf{kl}} \sin 2\theta_{\mathbf{k}} \sin 2\theta_{\mathbf{l}}, \tag{2.44}$$

we can perform minimization using θ as the parameter, then

$$\frac{\partial}{\partial\theta_{\mathbf{k}}}\langle\psi_G|\mathcal{H}-\mu N|\psi_G\rangle = 0 = -2\xi_{\mathbf{k}}\sin 2\theta_{\mathbf{k}} + \sum_{\mathbf{l}} V_{\mathbf{kl}}\cos\theta_{\mathbf{k}}\sin\theta_{\mathbf{l}}. \tag{2.45}$$

By organizing terms we get

$$\tan 2\theta_{\mathbf{k}} = \frac{\sum_{\mathbf{l}} V_{\mathbf{kl}} \sin 2\theta_{\mathbf{l}}}{2\xi_{\mathbf{k}}}. \tag{2.46}$$

Let us define the quantities

$$\Delta_{\mathbf{k}} = -\sum_{\mathbf{l}} V_{\mathbf{kl}} u_{\mathbf{l}} v_{\mathbf{k}} = -\frac{1}{2}\sum_{\mathbf{l}} V_{\mathbf{kl}} \sin 2\theta_{\mathbf{l}} \tag{2.47}$$

and

$$E_{\mathbf{k}} = (\Delta_{\mathbf{k}}^2 + \xi_{\mathbf{k}}^2)^{1/2}. \tag{2.48}$$

For now, it might seem some random definition, but later it will acquire a physical significance as the energy-gap parameter and quasi-particle excitation energy, respectively). Then 2.46 becomes

$$\tan 2\theta_k = -\frac{\Delta_{\mathbf{k}}}{\xi_{\mathbf{k}}} \tag{2.49}$$

and noticing that by

$$E_{\mathbf{k}} = \begin{cases} |\Delta_{\mathbf{k}}|\left(1+\frac{\xi_{\mathbf{k}}^2}{\Delta_{\mathbf{k}}^2}\right)^{1/2} = \frac{\Delta_{\mathbf{k}}}{\sin 2\theta_{\mathbf{k}}} \\ |\xi_{\mathbf{k}}|\left(1+\frac{\Delta_{\mathbf{k}}^2}{\xi_{\mathbf{k}}^2}\right)^{1/2} = -\frac{\xi_{\mathbf{k}}}{\cos 2\theta_k}, \end{cases} \tag{2.50}$$

we can conclude that

$$2u_{\mathbf{k}}v_{\mathbf{k}} = \sin 2\theta_{\mathbf{k}} = \frac{\Delta_{\mathbf{k}}}{E_{\mathbf{k}}} \tag{2.51}$$

and

$$v_{\mathbf{k}}^2 - u_{\mathbf{k}}^2 = \cos 2\theta_{\mathbf{k}} = -\frac{\xi_{\mathbf{k}}}{E_{\mathbf{k}}}. \tag{2.52}$$

where in the equations above we have fixed the sign for the sine and cosine in a way that $v_{\mathbf{k}}^2 \to 0$ as $\xi_{\mathbf{k}} \to \infty$, as it should be for a reasonable solution. Substituting the equations above into 2.46, we obtain the self-consistent equation

$$\Delta_{\mathbf{k}} = -\frac{1}{2}\sum_{\mathbf{l}} \frac{\Delta_{\mathbf{l}}}{E_{\mathbf{l}}} V_{\mathbf{kl}} = -\frac{1}{2}\sum_{\mathbf{l}} \frac{\Delta_{\mathbf{l}}}{(\Delta_{\mathbf{l}}^2 + \xi_{\mathbf{l}}^2)^{1/2}} V_{\mathbf{kl}}. \tag{2.53}$$

Of course $\Delta_{\mathbf{k}} = 0$ is a possible solution, a trivial one. We expect that the system have a non trivial solution with lower energy if $V_{\mathbf{kl}}$ is negative. We retain the model of $V_{\mathbf{kl}}$ used by cooper and by BCS in 2.9.

$$V_{\mathbf{kl}} = \begin{cases} -V \quad \text{if} \quad |\xi_{\mathbf{k}}| \quad \text{and} \quad |\xi_{\mathbf{l}}| \leq \hbar\omega_c \\ \\ 0 \quad \text{otherwise,} \end{cases} \tag{2.54}$$

with V being a positive constant. It is important to notice that in equation 2.9, it actually suggests that the relevant energy is $|\xi_{\mathbf{k}} - \xi_{\mathbf{l}}|$, the energy change of the electron in the scattering process, but to get a simple solution it is necessary to make a stronger restriction just like above. Inserting this in $V_{\mathbf{kl}}$ in 2.47, we find that it is satisfied by

$$\Delta_{\mathbf{k}} = \begin{cases} \Delta \quad \text{for} \quad |\xi_{\mathbf{k}}| < \hbar\omega_c \\ \\ 0 \quad \text{for} \quad |\xi_{\mathbf{k}}| > \hbar\omega_c. \end{cases} \tag{2.55}$$

In this model, $\Delta_{\mathbf{k}} = \Delta$, independent of $\mathbf{k}$. we can cancel it from both sides of 2.47, and our condition for self-consistency then reads

$$1 = \frac{V}{2}\sum_{\mathbf{k}} \frac{1}{E_{\mathbf{k}}}. \tag{2.56}$$

In the continuum limit, we can replace the summation for an integration from $-\hbar\omega_c$ to $\hbar\omega_c$, and using the symmetry of $\pm\xi$ values, we get

$$\frac{1}{N(0)V} = \int_0^{\hbar\omega_c} \frac{d\xi}{(\Delta^2 + \xi^2)^{1/2}} = \sinh^{-1}\frac{\hbar\omega_c}{\Delta}, \tag{2.57}$$

quite similar to what is done in section 2.1. Rearranging terms produces

$$\Delta = \frac{\hbar\omega_c}{\sinh\left[1/N(0)V\right]} \approx 2\hbar\omega_c e^{-1/N(0)V}. \tag{2.58}$$

Assuming in the last step that we are in the weak coupling limit $N(0)V \ll 1$.

It is quite straightforward to obtain the amplitudes with equations 2.49 to 2.52 and the normalization condition $u_{\mathbf{k}}^2 + v_{\mathbf{k}}^2 = 1$:

$$v_{\mathbf{k}}^2 = \frac{1}{2}\left(1 - \frac{\xi_{\mathbf{k}}}{E_{\mathbf{k}}}\right) = \frac{1}{2}\left[1 - \frac{\xi_{\mathbf{k}}}{(\Delta^2 + \xi_{\mathbf{k}}^2)^{1/2}}\right] \tag{2.59}$$

while

$$u_{\mathbf{k}}^2 = \frac{1}{2}\left(1 + \frac{\xi_{\mathbf{k}}}{E_{\mathbf{k}}}\right) = 1 - v_{\mathbf{k}}^2. \tag{2.60}$$

2.5 APPROACH VIA CANONICAL TRANSFORMATIONQ

In order to approach excited states, it is necessary to use a different method to get a reasonable solution. An alternate method is use the self-consistent method but without using any variational calculation.

We know already that the characteristic BCS pair-interaction hamiltonian 2.42 will lead to a ground state which some phase-coherent superposition of many-body state with pairs of states ($\mathbf{k}\uparrow$, $-\mathbf{k}\downarrow$) occupied or unoccupied as units. Because of the coherence, operators such as $c_{-\mathbf{k}\downarrow}c_{\mathbf{k}\uparrow}$ can have nonzero expectation values, since it connects many particle states with different number of particles. This effect is different from a normal metal where averaging such kind of operator gives us zero. Because of the large number of particles involved, the fluctuations about these expectation values are small. We can express such product of operators as

$$c_{-\mathbf{k}\downarrow}c_{\mathbf{k}\uparrow} = \langle c_{-\mathbf{k}\downarrow}c_{\mathbf{k}\uparrow}\rangle + (c_{-\mathbf{k}\downarrow}c_{\mathbf{k}\uparrow} - \langle c_{-\mathbf{k}\downarrow}c_{\mathbf{k}\uparrow}\rangle), \tag{2.61}$$

that is, we say that our operator is its average value plus fluctuation. We must neglect quantities which are bilinear in the small fluctuation in the parenthesis. It is easy then to obtain the mean field Hamiltonian

$$\mathcal{H}_M = \sum_{\mathbf{k}\omega} \xi_{\mathbf{k}} c^\dagger_{\mathbf{k}\sigma}c_{\mathbf{k}\sigma} - \sum_{\mathbf{kl}} V_{\mathbf{kl}}(c^\dagger_{\mathbf{k}\uparrow}c^\dagger_{-\mathbf{k}\downarrow}\langle c_{-\mathbf{l}\downarrow}c_{\mathbf{l}\uparrow}\rangle + \langle c_{-\mathbf{k}\downarrow}c_{\mathbf{k}\uparrow}\rangle^* c_{-\mathbf{l}\downarrow}c_{\mathbf{l}\uparrow} - \langle c_{-\mathbf{k}\downarrow}c_{\mathbf{k}\uparrow}\rangle^*\langle c_{-\mathbf{l}\downarrow}c_{\mathbf{l}\uparrow}\rangle). \tag{2.62}$$

The hamiltonian above is simpler due to the suppression of product of 4 operators. It has only states that connects one-particle states. However, it is important to notice the self-consistent nature that emerged from mean-field. Also, it does not conserve the number of particles. We can handle this situation by introducting a chemical potential μ to fix $\overline{N}$ at any desired value.

Let us now define

$$\Delta_{\mathbf{k}} = -\sum_{\mathbf{l}} V_{\mathbf{kl}}\langle c_{-\mathbf{l}\downarrow}c_{\mathbf{l}\uparrow}\rangle, \tag{2.63}$$

which is very similar to the definition of 2.47, and it turn out to give the gap in the energy spectrum. Writing the Mean-field Hamiltonian in terms of the definition above we obtain

$$\mathcal{H}_M = \sum_{\mathbf{k}\omega} \xi_{\mathbf{k}} c^\dagger_{\mathbf{k}\sigma}c_{\mathbf{k}\sigma} - \sum_{\mathbf{k}}(\Delta_{\mathbf{k}} c^\dagger_{\mathbf{k}\uparrow}c^\dagger_{-\mathbf{k}\downarrow} + \Delta^*_{\mathbf{k}} c_{-\mathbf{k}\downarrow}c_{\mathbf{k}\uparrow} - \Delta_{\mathbf{k}}\langle c_{-\mathbf{k}\downarrow}c_{\mathbf{k}\uparrow}\rangle^*). \tag{2.64}$$

The Hamiltonian above can be diagonalized by a appropriate linear transformation:

$$\begin{aligned} c_{\mathbf{k}\uparrow} &= u^*_{\mathbf{k}}\gamma_{\mathbf{k}\,\mathbf{0}} + v_{\mathbf{k}}\gamma^\dagger_{\mathbf{k}\,\mathbf{1}}, \\ c^\dagger_{-\mathbf{k}\downarrow} &= -v^*_{\mathbf{k}}\gamma_{\mathbf{k}0} + u_{\mathbf{k}}\gamma^\dagger_{\mathbf{k}1}. \end{aligned} \tag{2.65}$$

The coefficients are the same amplitudes from previous section and they satisfy $|u_{\mathbf{k}}|^2+|v_{\mathbf{k}}|^2=1$ and $\gamma_{\mathbf{k}}$ are new Fermi operators. We can interpret the new operators as follow: $\gamma_{\mathbf{k}0}$ destroys an electron with $\mathbf{k}\uparrow$ or creating an electron with $-\mathbf{k}\downarrow$; in both cases, the resultant effect is decrease the system momentum by $\mathbf{k}$ and reduce S_z by $\hbar$. This can be seen by inverting the linear transformation above. Similar properties appear for the other three operators.

By substituting the old for the new Fermi operators, and using the fermionic properties like keeping creation operators to the left and destruction operators to the right using commutation relations, after a lengthy calculation, we obtain the following Hamiltonian

$$\begin{aligned}\mathcal{H}_M =&\sum_{\mathbf{k}}\xi_{\mathbf{k}}[(|u_{\mathbf{k}}|^2-|v_{\mathbf{k}}|^2)(\gamma^\dagger_{\mathbf{k}0}\gamma_{\mathbf{k}0}+\gamma^\dagger_{\mathbf{k}1}\gamma_{\mathbf{k}1})+2|v_{\mathbf{k}}|^2+2u^*_{\mathbf{k}}v^*_{\mathbf{k}}\gamma_{\mathbf{k}1}\gamma_{\mathbf{k}0}\\ &+2u_{\mathbf{k}}v_{\mathbf{k}}\gamma^\dagger_{\mathbf{k}0}\gamma^\dagger_{\mathbf{k}1}]+\sum_{\mathbf{k}}[(\Delta_{\mathbf{k}}u_{\mathbf{k}}v^*_{\mathbf{k}}+\Delta^*_{\mathbf{k}}u^*_{\mathbf{k}}v_{\mathbf{k}})(\gamma^\dagger_{\mathbf{k}0}\gamma_{\mathbf{k}0}+\gamma^\dagger_{\mathbf{k}1}\gamma_{\mathbf{k}1}-1)\\ &(\Delta_{\mathbf{k}}v^{*2}_{\mathbf{k}}-\Delta^*_{\mathbf{k}}u^{*2}_{\mathbf{k}})\gamma_{\mathbf{k}1}\gamma_{\mathbf{k}0}+(\Delta^*_{\mathbf{k}}v^2_{\mathbf{k}}-\Delta_{\mathbf{k}}u^2_{\mathbf{k}})\gamma^\dagger_{\mathbf{k}0}\gamma^\dagger_{\mathbf{k}1}+\Delta_{\mathbf{k}}\langle c_{-\mathbf{k}\downarrow}c_{\mathbf{k}\uparrow}\rangle^*]\end{aligned} \tag{2.66}$$

we have o choose $u_{\mathbf{k}}$ and $v_{\mathbf{k}}$ in order to make coefficients $\gamma_{\mathbf{k}1}\gamma_{\mathbf{k}0}$ and $\gamma^\dagger_{\mathbf{k}0}\gamma^\dagger_{\mathbf{k}1}$ vanish, so that the hamiltonian will be diagonalized. Gathering all terms that are together with the operators above, we obtain the following relation :

$$2\xi_{\mathbf{k}}u_{\mathbf{k}}v_{\mathbf{k}}+\Delta^*_{\mathbf{k}}v^2_{\mathbf{k}}-\Delta_{\mathbf{k}}u^2_{\mathbf{k}}=0, \tag{2.67}$$

solving for the ratio $v_{\mathbf{k}}/u_{\mathbf{k}}$ yields

$$\frac{v_{\mathbf{k}}}{u_{\mathbf{k}}}=\frac{\sqrt{\xi^2_{\mathbf{k}}+|\Delta^2_{\mathbf{k}}|}-\xi_{\mathbf{k}}}{\Delta^*_{\mathbf{k}}}, \tag{2.68}$$

where we choose only the positive root to ensure that the energy of the BCS state is a minimum and not a maximum. Notice that since the numerator is a real number, the phase of $\Delta_{\mathbf{k}}$ must be the same as the relative phase between $v_{\mathbf{k}}$ and $u_{\mathbf{k}}$. We can set the phase of $u_{\mathbf{k}}$ to be zero without loss of generality, it follows that the phases of $v_{\mathbf{k}}$ and $\Delta_{\mathbf{k}}$ are the same. Given the normalization requirement that $|u_{\mathbf{k}}|^2+|v_{\mathbf{k}}|^2=1$ and solving for the coefficients we find

$$|v_{\mathbf{k}}|^2=1-|u_{\mathbf{k}}|^2=\frac{1}{2}\left(1-\frac{\xi_{\mathbf{k}}}{E_{\mathbf{k}}}\right), \tag{2.69}$$

where we have assigned $E_{\mathbf{k}}=(\xi^2_{\mathbf{k}}+|\Delta_{\mathbf{k}}|^2)^{1/2}$. This is the same result as obtained from variational method.

By having chosen the the amplitudes $u_{\mathbf{k}}$ and $v_{\mathbf{k}}$ to be diagonalize the hamiltonian, the remaining terms reduce the hamiltonian to

$$\mathcal{H}_M=\sum_{\mathbf{k}}(\xi_{\mathbf{k}}-E_{\mathbf{k}}+\Delta_{\mathbf{k}}\langle c_{-\mathbf{k}\downarrow}c_{\mathbf{k}\uparrow}\rangle^*)+\sum_{\mathbf{k}}E_{\mathbf{k}}(\gamma^\dagger_{\mathbf{k}0}\gamma_{\mathbf{k}0}+\gamma^\dagger_{\mathbf{k}1}\gamma_{\mathbf{k}1}). \tag{2.70}$$

The first term in the hamiltonian is constant and differs from the corresponding sum for the normal state at T = 0 by exactly the condensation energy as seen before. The second sum gives us increase in energy aboce the gound state in terms of the new number operator $\gamma^\dagger_{bfk}\gamma_{\mathbf{k}}$. Since now our new hamiltonian resembles a ideal gas hamiltonian once it is diagonalized, we can say that $\gamma_{\mathbf{k}}$ describe an elementary quasi-particle excitation of the system, which are often called Bogolons. The excitation is $E_{\mathbf{k}}$ as seen in the hamiltonian, and as said before, $\Delta_{\mathbf{k}}$ is the energy gap or minimum excitation energy, that is, even at Fermi surface where $\xi_{\mathbf{k}} = 0$, $E_{\mathbf{k}} = |\Delta_{\mathbf{k}}| > 0$.

Of course, we are not over yet because our self-consistent problem is not fully determined in terms of the amplitudes and energies found above. In fact, the gap remains unknown

$$\Delta_{\mathbf{k}} = -\sum_{\mathbf{l}} V_{\mathbf{kl}} u^*_{\mathbf{l}} v_{\mathbf{l}} \langle c_{-\mathbf{l}\downarrow} c_{\mathbf{l}\uparrow}\rangle = -\sum_{\mathbf{l}} V_{\mathbf{kl}} u^*_{\mathbf{l}} v_{\mathbf{l}} \langle 1 - \gamma^*_{\mathbf{l}0}\gamma_{\mathbf{l}0} - \gamma^*_{\mathbf{l}1}\gamma_{\mathbf{l}1}\rangle. \tag{2.71}$$

At T = 0, the system has no excitations and we return 2.47. In fact, as we increase temperature an more excitations are added to the system, there must be a better way to calculate the new gap as a function of temperature, as we shall see in the following section

Before we go further, let us calculate the ground state wavefunction using the current method. We know that the ground state has to satisfy the condition

$$\gamma_{\mathbf{k}\sigma}|\psi_G\rangle = 0, \tag{2.72}$$

using the inverse linear transformation 2.65, we can write the last equation as

$$u_{\mathbf{k}} c_{\mathbf{k}\uparrow}|\psi_G\rangle = v_{\mathbf{k}} c^\dagger_{-\mathbf{k}\downarrow}|\psi_G\rangle, \tag{2.73}$$

since we know already that the state is coherent, it is reasonable to propose an ansatz as a power of cooper pairs

$$|\psi_G\rangle = \mathcal{N}\prod_{\mathbf{q}} e^{\alpha_{\mathbf{q}} c^\dagger_{\mathbf{q}\uparrow} c^\dagger_{-\mathbf{q}\downarrow}}|0\rangle, \tag{2.74}$$

$\mathcal{N}$ is a normalization constant that will be determined later. To simplify the notation let us call the exponent in the exponential operator as $\theta_{\mathbf{k}} = \alpha_{\mathbf{q}} c^\dagger_{\mathbf{q}\uparrow} c^\dagger_{-\mathbf{q}\downarrow}$. To understand how $c_{\mathbf{k}\uparrow}$ and $c^\dagger_{-\mathbf{k}\downarrow}$ acts on the exponential operator, we must understand how it commutes with the exponent. Since the operators can easily be swapped places when $\mathbf{q} \neq \mathbf{k}$, let us only consider when $\mathbf{q} = \mathbf{k}$, we have

$$c_{\mathbf{k}\uparrow} e^{\theta_{\mathbf{k}}} = \sum_{n=1}^{\infty} \frac{c_{\mathbf{k}\uparrow}\theta^n_{\mathbf{k}}}{n!}|0\rangle. \tag{2.75}$$

Using commutation relations

$$[c_{\mathbf{k}\uparrow}, \theta_{\mathbf{k}}] = \alpha_{\mathbf{k}}\left\{c_{\mathbf{k}\uparrow}, c^\dagger_{\mathbf{k}\uparrow}\right\} c^\dagger_{-\mathbf{k}\downarrow} = \alpha_{\mathbf{k}} c^\dagger_{-\mathbf{k}\downarrow}. \tag{2.76}$$

Actually, it is possible to how that, in general, any function of operators $f(c^\dagger_{\mathbf{k}\uparrow})$ commuting with its operator parameter $c_{\mathbf{k}\uparrow}$ can be expressed as a derivative

$$\left[c_{\mathbf{k}\uparrow}, f(c^\dagger_{\mathbf{k}\uparrow})\right] = f'(c^\dagger_{\mathbf{k}\uparrow}). \tag{2.77}$$

In our case, we want to know how to commute $c_{\mathbf{k}\uparrow}$ with $\theta^n_{\mathbf{k}}$, which is also a function of $c_{\mathbf{k}\uparrow}$, so the chain rule is valid and we easily obtain

$$[c_{\mathbf{k}\uparrow}, \theta^n_{\mathbf{k}}] = \frac{d\theta^n_{\mathbf{k}}}{dc_{\mathbf{k}\uparrow}} = n\theta^{n-1}_{\mathbf{k}} [c_{\mathbf{k}\uparrow}, \theta_{\mathbf{k}}] = n\theta^{n-1}_{\mathbf{k}} \alpha_{\mathbf{k}} c^\dagger_{-\mathbf{k}\downarrow}. \tag{2.78}$$

Applying $|0\rangle$ both sides in equation above and assuming that $c_{\mathbf{k}\uparrow}|0\rangle = 0$ we obtain

$$c_{\mathbf{k}\uparrow}\theta^n_{\mathbf{k}} = n\theta^{n-1}_{\mathbf{k}} \alpha_{\mathbf{k}} c^\dagger_{-\mathbf{k}\downarrow}. \tag{2.79}$$

Therefore, we have

$$c_{\mathbf{k}\uparrow} e^{\alpha_{\mathbf{k}} c^\dagger_{\mathbf{k}\uparrow} c^\dagger_{-\mathbf{k}\downarrow}} |0\rangle = \alpha_{\mathbf{k}} \sum_{n=1}^{\infty} \frac{\theta^{n-1}_{\mathbf{k}}}{(n-1)!} c^\dagger_{-\mathbf{k}\downarrow}|0\rangle. \tag{2.80}$$

Besides, for the creation operator $c^\dagger_{-\mathbf{k}\downarrow}$

$$\left[\theta_{\mathbf{k}}, c^\dagger_{-\mathbf{k}\downarrow}\right] = \alpha \left[c^\dagger_{\mathbf{k}\uparrow} c^\dagger_{-\mathbf{k}\downarrow}, c^\dagger_{-\mathbf{k}\downarrow}\right] = 0, \tag{2.81}$$

then 2.80 can be written as

$$c_{\mathbf{k}\uparrow} e^{\alpha_{\mathbf{k}} c^\dagger_{\mathbf{k}\uparrow} c^\dagger_{-\mathbf{k}\downarrow}} |0\rangle = \alpha_{\mathbf{k}} c^\dagger_{-\mathbf{k}\downarrow} \sum_{n=1}^{\infty} \frac{\theta^{n-1}_{\mathbf{k}}}{(n-1)!}|0\rangle = \alpha_{\mathbf{k}} c^\dagger_{-\mathbf{k}\downarrow} e^{\alpha_{\mathbf{k}} c^\dagger_{\mathbf{k}\uparrow} c^\dagger_{-\mathbf{k}\downarrow}}|0\rangle. \tag{2.82}$$

Then substituting in 2.73 we see that

$$u_{\mathbf{k}} c_{\mathbf{k}\uparrow}|\psi_G\rangle = u_{\mathbf{k}} \alpha_{\mathbf{k}} c^\dagger_{-\mathbf{k}}|\psi_G\rangle = v_{\mathbf{k}} c^\dagger_{-\mathbf{k}\downarrow}|\psi_G\rangle, \tag{2.83}$$

we can see that $\alpha_{\mathbf{k}}$ has the value

$$\alpha_{\mathbf{k}} = \frac{v_{\mathbf{k}}}{u_{\mathbf{k}}}. \tag{2.84}$$

Hence, the BCS ground state wavefunction is

$$\begin{aligned} |\psi_G\rangle =& \mathcal{N} \prod_{\mathbf{k}} e^{\frac{v_{\mathbf{k}}}{u_{\mathbf{k}}} c^\dagger_{\mathbf{k}\uparrow} c^\dagger_{-\mathbf{k}\downarrow}} |0\rangle \\ =& \mathcal{N} \prod_{\mathbf{k}} \left(1 + \frac{v_{\mathbf{k}}}{u_{\mathbf{k}}} c^\dagger_{\mathbf{k}\uparrow} c^\dagger_{-\mathbf{k}\downarrow}\right) |0\rangle. \end{aligned} \tag{2.85}$$

From the first to second equality we used the fact that operating $c^\dagger$ twice or more results in zero from Pauli's exclusion principle.

Normalizing the wavefunction is a easy task compared to before, just swapping creation operators to the left and destruction to the right:

$$\begin{aligned}\langle 0|(u_{\mathbf{k}}^{*}+v_{\mathbf{k}}^{*}c_{\mathbf{k}\uparrow}c_{-\mathbf{k}\downarrow})(u_{\mathbf{k}}+v_{\mathbf{k}}c_{\mathbf{k}\uparrow}^{\dagger}c_{-\mathbf{k}\downarrow}^{\dagger})|0\rangle &= \langle 0||u_{\mathbf{k}}|^{2}+|v_{\mathbf{k}}|^{2}c_{\mathbf{k}\uparrow}c_{\mathbf{k}\uparrow}^{\dagger}c_{-\mathbf{k}\downarrow}c_{-\mathbf{k}\downarrow}^{\dagger}|0\rangle \\ &= \langle 0|(|u_{\mathbf{k}}|^{2}+|v_{\mathbf{k}}|^{2})|0\rangle,\end{aligned} \tag{2.86}$$

which is equal to 1, then, we can easily conclude that $\mathcal{N}=1$, so the normalized BCS wavefunction is given by

$$|\psi_{G}\rangle=\prod_{\mathbf{k}}(u_{\mathbf{k}}+v_{\mathbf{k}}c_{\mathbf{k}\uparrow}^{\dagger}c_{-\mathbf{k}\downarrow}^{\dagger})|0\rangle. \tag{2.87}$$

2.6 FINITE TEMPERATURE

We have identified $E_{\mathbf{k}}$ as the excitation energy for a fermionic quasi-particle. We known from statistical mechanics that the excitation in thermal equilibrium is given by the Fermi-Dirac distribution

$$f(E_{\mathbf{k}})=(e^{\beta E_{\mathbf{k}}}+1)^{-1}, \tag{2.88}$$

then the new operators $\gamma_{\mathbf{k}}$ and $\gamma_{\mathbf{k}}^{\dagger}$ satisfies fermionic statistical averages in such a way that we have

$$\langle 1-\gamma_{\mathbf{k}0}^{\dagger}\gamma_{\mathbf{k}0}-\gamma_{\mathbf{k}1}^{\dagger}\gamma_{\mathbf{k}1}\rangle=1-2f(E_{\mathbf{k}}), \tag{2.89}$$

since the product $\gamma^{\dagger}\gamma$ plays a hole of number operator for Bogolons. In general, 2.71 becomes

$$\begin{aligned}\Delta_{\mathbf{k}} &= -\sum_{\mathbf{l}}V_{\mathbf{k}\,\mathbf{l}}u_{\mathbf{l}}^{*}v_{\mathbf{l}}[1-2f(E_{\mathbf{k}})] \\ &= -\sum_{\mathbf{l}}V_{\mathbf{k}\,\mathbf{l}}\frac{\Delta_{\mathbf{l}}}{2E_{\mathbf{l}}}\tanh\frac{\beta E_{\mathbf{l}}}{2},\end{aligned} \tag{2.90}$$

where the second equality was used 2.69 By making the BCS approximation that $V_{\mathbf{k}\,\mathbf{l}}=-V$, we have $\Delta_{\mathbf{k}}=\Delta_{\mathbf{l}}=\Delta$, and the self-consistentent condition becomes

$$\frac{1}{V}=\frac{1}{2}\sum_{\mathbf{k}}\frac{\tanh(\beta E_{\mathbf{k}}/2)}{E_{\mathbf{k}}}, \tag{2.91}$$

where $E_{\mathbf{k}}=(\xi_{\mathbf{k}}^{2}+\Delta^{2})^{1/2}$. With this procedure we are able to determine how the gap evolves as we increase the temperature.

To determine the critical temperature, which is the temperature at which the order parameter vanishes, we make the assumption that $E_{\mathbf{k}}\to|\xi_{\mathbf{k}}|$, where the excitation spectrum becomes the same as in the normal state. By converting the summation in equation 2.91 into

an integral, we obtain:

$$\frac{1}{N(0)V} = \int_0^{\hbar\omega_D} \frac{d\epsilon}{\epsilon} \tanh\left(\frac{\epsilon}{2k_BT_c}\right) = \int_0^{\frac{\hbar\omega_D}{2k_BT_c}} dx \frac{\tanh x}{x}, \tag{2.92}$$

the integral is not trivial to solve, we perform it by parts using the fact that $\hbar\omega_D \gg k_BT_c$:

$$\int_0^{\frac{\hbar\omega_D}{2k_BT_c}} dx \frac{\tanh x}{x} \approx (\tanh x \ln x)_0^{\frac{\hbar\omega_D}{2k_BT_c}} - \int_0^{\infty} dx \frac{\ln x}{\cosh^2 x} \tag{2.93}$$

the last integral can be connected with Euler-Mascheroni constant (γ_E)

$$\begin{aligned} &(\tanh x \ln x)_0^{\frac{\hbar\omega_D}{2k_BT_c}} - \int_0^{\infty} dx \frac{\ln x}{\cosh^2 x} \\ &\approx \ln\left(\frac{\hbar\omega_D}{2k_BT_c}\right) - \ln\left(\frac{\pi}{4e^{\gamma_E}}\right) \\ &\approx \ln\left(\frac{2e^{\gamma_E}\hbar\omega_D}{\pi k_BT_c}\right). \end{aligned} \tag{2.94}$$

Then we conclude that the critical temperature is

$$T_c = \frac{2e^{\gamma_E}}{\pi} \frac{\hbar\omega_D}{k_B} e^{-\frac{1}{VN(0)}}. \tag{2.95}$$

Using 2.58 we have one of the most impressive predictions of BCS theory

$$\Delta(T=0) = 1.76 k_BT_c. \tag{2.96}$$

This relation holds approximately for most known superconductors. The BCS theory also addresses the Isotope Effect, which demonstrates the linear dependence of T_c on ω_D. This dependence varies inversely with the square root of the ionic mass M, such that $T_c \propto \omega_D \propto M^{-1/2}$. Experimental observations support this relation, establishing a connection between superconductivity and electron-phonon interactions as the primary cause (TINKHAM, 2004) (BRUUS; FLENSBERG, 2004).

To calculate the temperature dependence of the superconducting energy gap in BCS theory, we solve the self-consistent equation 2.91 iteratively until convergence is achieved. This numerical approach yields a plot, as shown in the following image:

In weak-coupling superconductors, characterized by $\hbar\omega_c/k_BT_c \gg 1$, the ratio $\Delta(T)/\Delta(0)$ becomes a universal function of T/T_c. This function monotonically decreases from 1 at $T = 0$ to 0 at T_c. Near absolute zero, the temperature variation is exponentially slow, with $e^{-\Delta/k_BT} \approx 0$. Consequently, the hyperbolic tangent function is nearly equal to 1 and insensitive to temperature. As the temperature approaches T_c, $\Delta(T)$ exhibits a rapid drop to zero, with a tangent that becomes vertical. Approximately, we have:

$$\frac{\Delta(T)}{\Delta(0)} \approx 1.74\left(1 - \frac{T}{T_c}\right)^{1/2} \quad T \approx T_c. \tag{2.97}$$

This kind of variation of the order parameter with square root of $(T_c - T)$ is characteristic of all mean-field theories such as molecular-field theory of ferromagnetism.

3 THE BOGOLIUBOV DE GENNES EQUATION

3.1 INTRODUCTION

The Bogoliubov-de Gennes (BdG) theory is a mathematical framework used to describe superconductivity in condensed matter systems, particularly in the context of tight-binding models. It was developed by Bogoliubov. Gorkov developed method based on Green functions.

The tight-binding model is a powerful framework used in condensed matter physics to describe the electronic structure of solids. It assumes that the behavior of electrons in a crystal lattice can be approximated by considering their interactions only with their nearest neighboring atoms. In this model, the electronic wavefunction is constructed as a linear combination of atomic wavefunctions centered around each lattice site. The hopping parameters between neighboring sites dictate the probability of electron movement, capturing the effects of band formation and electronic transport properties. By incorporating the appropriate energy levels and interactions, the tight-binding model enables the analysis of various phenomena such as band structures, electronic conductivity, and electronic states in crystalline materials. (KITTEL, 2004).

The BdG theory extends the concept of a single-particle wavefunction to include both particle-like and hole-like excitations. It introduces a set of quasiparticle operators, called Bogoliubov operators, which are linear combinations of creation and annihilation operators for electrons and holes, just like we have developed in the previous chapter. These operators diagonalize the Hamiltonian of the system and provide a convenient representation for describing superconductivity.

The BdG theory differs from the BCS (Bardeen-Cooper-Schrieffer) theory, which was developed earlier and is another important framework for understanding superconductivity. While both theories describe superconductivity, they approach the problem from different perspectives.

The BCS theory focuses on the macroscopic wave function of the superconducting state, describing it as a coherent condensate of Cooper pairs. It introduces the concept of the BCS wave function, which is a linear combination of electron pairs in a superposition of different momentum states. The BCS theory explains the pairing mechanism by the exchange of virtual phonons, leading to the formation of bound states with net attractive interactions.

On the other hand, the BdG theory provides description of superconductivity by explicitly

including both electrons and holes as quasiparticles in real space, thus making possible consider inhomogeneities of spacial structure like impurities, finite size effects and so on. In such cases BCS theory is less applicable.

3.2 HUBBARD MODEL

The Hubbard model is a mathematical model used to describe interacting electrons in a lattice. It was introduced by John Hubbard in the 1960s and has since become a cornerstone of condensed matter physics, particularly in the study of strongly correlated systems. The Hubbard model captures the interplay between electron-electron interactions and the lattice structure, making it a powerful tool for investigating a wide range of phenomena, including superconductivity (OREG, Y., 2018).

In the context of the Bogoliubov-de Gennes (BdG) equation, the Hubbard model is often used as a starting point to describe the electronic properties of materials, especially in the presence of strong electron-electron interactions. The BdG equation, which incorporates both single-particle and pairing effects, provides a means to study the emergence of superconductivity in such systems.

To apply the Hubbard model to the BdG equation, we consider a lattice with sites labeled by index i. The Hubbard Hamiltonian can be written as:

$$H_{\text{Hubbard}} = -\sum_{ij\sigma} t_{ij} c^{\dagger}_{i\sigma} c_{j\sigma} + U \sum_{i} n_{i\uparrow} n_{i\downarrow}, \tag{3.1}$$

where t_{ij} represents the hopping integral between sites i and j, $c^{\dagger}_{i\sigma}$ and $c_{i\sigma}$ are the creation and annihilation operators for an electron with spin σ at site i, U represents the on-site Coulomb interaction, and $n_{i\sigma} = c^{\dagger}_{i\sigma} c_{i\sigma}$ is the number operator.

To incorporate superconductivity within the Hubbard model, one can introduce an additional term that represents the attractive electron-electron interactions responsible for pairing. This pairing term can take different forms, such as an on-site attractive potential or an effective attractive interaction mediated by phonons or other mechanisms.

The Hubbard model with superconducting pairing interactions can be analyzed using the BdG formalism. The BdG equations, which are derived by introducing a Bogoliubov transformation to diagonalize the Hamiltonian, provide a means to determine the energy spectrum, wavefunctions, and other properties of the quasiparticle excitations in the system.

By solving the BdG equations within the framework of the Hubbard model, researchers can explore various aspects of superconductivity, including the formation of Cooper pairs, the energy gap, the critical temperature, and the effects of interactions on the superconducting properties. The Hubbard model offers a valuable tool for understanding the interplay between electron-electron interactions, lattice structure, and superconductivity, especially in systems with strong correlations.

In summary, the Hubbard model serves as a foundation for investigating the electronic properties of materials with strong electron-electron interactions. When combined with the BdG equations, it enables the study of superconductivity, providing insights into the emergence and behavior of quasiparticle excitations and other properties related to superconducting states in correlated systems.

3.3 DERIVATION OF BDG EQUATIONS

The Hubbard Model poses significant challenges in manipulating due to the exponential number of possible configurations, with 2^N configurations for N electrons considered within a 2-particle Fock space. However, these complexities can be alleviated by employing mean-field theory within the Hubbard Hamiltonian, leading to the generation of a self-consistent 2N Hamiltonian. Similarly to the previous section, after applying mean-field theory, the appropriate transformation in the Hamiltonian operators must be sought to map the problem onto a free particle Hamiltonian known as the Bogolons Hamiltonian. Determining the coefficients of this transformation lies at the heart of the Bogoliubov-de Gennes theory. In essence, the main focus is on finding eigenvalues and energies of a less intricate Hamiltonian, simplifying the analysis of the Hubbard Model and facilitating the exploration of its electronic properties (ZHU, 2016).

Let us start with the Hubbard Hamiltonian adding the chemical potential and a possible non-magnetic impurity:

$$H = H_0 - |U| \sum_i n_{i\uparrow} n_{i\downarrow}, \tag{3.2}$$

where

$$H_0 = -t \sum_{\langle ij \rangle, \sigma} (c^\dagger_{i\sigma} c_{j\sigma} + H.c.) + \sum_{i,\sigma} (V_i - \mu) n_{i,\sigma}. \tag{3.3}$$

H_0 is the single electron Hamiltonian, it contains all dynamics for a single electron and it would reproduce all known results for tight binding if U = 0. V_i is a disordered potential that will be explained better further but it is important to notice that it affects only one particle

states. The second term in Eq. 3.2 is an atractive potential for example due to the electron-phonon interaction which will reproduce the superconductivity - it is a 2-electron term. Such Hamiltonian, as said before, is extremely hard to handle. Let us apply a mean field theory on the interacting part:

$$\begin{aligned} n_{i\uparrow}n_{i\downarrow} = c^\dagger_{i\uparrow}c_{i\uparrow}c^\dagger_{i\downarrow}c_{i\downarrow} = \langle c^\dagger_{i\uparrow}c^\dagger_{i\downarrow}\rangle c_{i\downarrow}c_{i\uparrow} + c^\dagger_{i\uparrow}c^\dagger_{i\downarrow}\langle c_{i\downarrow}c_{i\uparrow}\rangle - \langle c^\dagger_{i\uparrow}c^\dagger_{i\downarrow}\rangle\langle c_{i\downarrow}c_{i\uparrow}\rangle \\ + \langle c^\dagger_{i\uparrow}c_{i\uparrow}\rangle c^\dagger_{i\downarrow}c_{i\downarrow} + c^\dagger_{i\uparrow}c_{i\uparrow}\langle c^\dagger_{i\downarrow}c_{i\downarrow}\rangle - \langle c^\dagger_{i\uparrow}c_{i\uparrow}\rangle\langle c^\dagger_{i\downarrow}c_{i\downarrow}\rangle, \end{aligned} \tag{3.4}$$

by defining the order parameter as $\Delta_i = -|U|\langle c_{i\downarrow}c_{i\uparrow}\rangle$ and remembering that $\langle n_{i\sigma}\rangle = \langle c^\dagger_{i\sigma}c_{i\sigma}\rangle$ the previous equation can be written as:

$$\begin{aligned} |U|n_{i\uparrow}n_{i\downarrow} = |U|c^\dagger_{i\uparrow}c_{i\uparrow}c^\dagger_{i\downarrow}c_{i\downarrow} = -\Delta^*_i c_{i\downarrow}c_{i\uparrow} - \Delta_i c^\dagger_{i\uparrow}c^\dagger_{i\downarrow} - \frac{|\Delta_i|^2}{|U|} \\ + |U|\langle n_{i\uparrow}\rangle n_{i\downarrow} + |U|\langle n_{i\downarrow}\rangle n_{i\uparrow} - |U|\langle n_{i\uparrow}\rangle\langle n_{i\downarrow}\rangle, \end{aligned} \tag{3.5}$$

The constant terms (with no operators) can be discarded since it is not going to be relevant to the development of the theory. Our mean field Hamiltonian then becomes

$$H_{MF} = \sum_{ij\sigma} c^\dagger_{i\sigma}h_{ij,\sigma}c_{j\sigma} + \sum_i [\Delta_i c^\dagger_{i\uparrow}c^\dagger_{i\downarrow} + \Delta^*_i c_{i\uparrow}c_{i\downarrow}], \tag{3.6}$$

where $h_{ij,\sigma}$ is redefined as the part where it contains all single particle terms, hoppings, chemical potential and so on.

The following commutation relations can be derived easily with basic commutation rules:

$$[c_{i\uparrow}, H_{MF}] = \sum_j h_{ij,\uparrow}c_{j\uparrow} + \Delta_i c^\dagger_{i\downarrow}, \tag{3.7a}$$

$$[c_{i\downarrow}, H_{MF}] = \sum_j h_{ij,\downarrow}c_{j\downarrow} - \Delta_i c^\dagger_{i\uparrow}. \tag{3.7b}$$

It is only necessary to keep in mind that since creation and annihilation operators are fermionic, it is necessary to connect commutators with anticommutators via

$$[A, BC] = \{A, B\}C - B\{A, C\}. \tag{3.8}$$

Now, in order to diagonalize the Hamiltonian, it is necessary to introduce the Bogolon operators through the canonical Bogoliubov transformation

$$c_{i\uparrow} = \sum_n{}' (u^n_i\gamma_{n\uparrow} - v^{n*}_i\gamma^\dagger_{n\downarrow}), \quad c_{i\downarrow} = \sum_n{}' (u^n_i\gamma_{n\downarrow} + v^{n*}_i\gamma^\dagger_{n\uparrow}), \tag{3.9}$$

quite similar to what was done in previous chapter, with $\sum_n |u^n_i|^2 + |v^n_i|^2 = 1$. The prime above summation indicates the summation is performed only over positive energies. The operators

above and their hermitian conjugates satisfies the fermion commutation relation

$$\begin{aligned}\{\gamma^{\dagger}_{n\alpha}, \gamma_{m\beta}\} &= \delta_{mn}\delta_{\alpha\beta},\\ \{\gamma_{n\alpha}, \gamma_{m\beta}\} &= 0.\end{aligned} \tag{3.10}$$

The transformation 3.9 diagonalizes H_{MF}, giving rise to

$$H_{MF} = E_g + \sum_{n,\alpha} E_n \gamma^{\dagger}_{n\alpha}\gamma_{n\alpha}, \tag{3.11}$$

where E_g is the ground state of H_{MF} and E_n is the energy of excitation n. As any usual non interaction Hamiltonian we can write the diagonalization condition of H_{MF} with

$$\begin{aligned}[H_{MF}, \gamma_{n\alpha}] &= -E_n\gamma_{n\alpha},\\ [H_{MF}, \gamma^{\dagger}_{n\alpha}] &= E_n\gamma^{\dagger}_{n\alpha}.\end{aligned} \tag{3.12}$$

To derive equations for u^n and v^n we must calculate the commutators 3.7a using the H_{MF} with the Bogolon operators. After applying that, we need only to compare coeficients of γ_n and $\gamma^{\dagger}_n$ on the two sides of the equation, we obtain the celebrated Bogoliubov-de Gennes Equations:

$$\begin{aligned}E_n u^n_i &= \sum_j h_{ij,\uparrow}u^n_j + \Delta_i v^n_i,\\ E_n v^n_i &= -\sum_j h^*_{ij,\downarrow}v^n_j + \Delta^*_i u^n_i.\end{aligned} \tag{3.13}$$

It is easy to show that if (u v) are solutions for BdG Equation with energy E, then ($-v^*$, u^*) is solution for energy -E. The idea is just multiply both equations above to -1 and use the complex conjugate.

The mean field theory approach makes necessary to calculate the self-consistent parameter Δ_i and $\langle n_{i\sigma}\rangle$. By using the Bogolon operators 3.9 we can write both quantities in terms of the amplitudes u and v. It is important to notice here that the averages performed here are in equilibrium with a thermal reservoir at temperature T

$$\begin{aligned}\Delta_i = -|U|\langle c_{i\downarrow}c_{i\uparrow}\rangle &= -|U|\sum_{m,n}{}'(\langle\gamma^{\dagger}_{n\uparrow}\gamma_{m\uparrow}\rangle u^n_i v^{m*}_i - \langle\gamma_{m\downarrow}\gamma^{\dagger}_{n\downarrow}\rangle u^m_i v^{n*}_i)\\ &= -|U|\sum_n{}'(u^n_i v^{n*}_i f(E_n) - u^n_i v^{n*}_i(1-f(E_E))\\ &= -|U|\sum_n{}' u^n_i v^{n*}_i \tanh\left(\frac{E_n}{2k_BT}\right),\end{aligned} \tag{3.14}$$

where we used the fact that

$$\langle\gamma^{\dagger}_{n\sigma}\gamma_{m\sigma'}\rangle = f(E_n)\delta_{mn}\delta_{\sigma\sigma'}. \tag{3.15}$$

$f(E_n)$ is the Fermi-Dirac distribution for the excitation energies. Very similar, the average number of particles is calculated

$$\begin{aligned}\langle n_{i\uparrow}\rangle &= \sum_n{}'(|u_i^n|^2\langle\gamma_{n\uparrow}^\dagger\gamma_{n\uparrow}\rangle + |v_i^n|^2\langle\gamma_{n\downarrow}\gamma_{n\downarrow}^\dagger\rangle)\\ &= \sum_n{}'[|u_i^n|^2 f(E_n) + |v_i^n|^2(1-f(E_n))],\end{aligned} \tag{3.16}$$

$$\begin{aligned}\langle n_{i\downarrow}\rangle &= \sum_n{}'(|u_i^n|^2\langle\gamma_{n\downarrow}^\dagger\gamma_{n\downarrow}\rangle + |v_i^n|^2\langle\gamma_{n\uparrow}\gamma_{n\uparrow}^\dagger\rangle)\\ &= \sum_n{}'[|u_i^n|^2 f(E_n) + |v_i^n|^2(1-f(E_n))].\end{aligned} \tag{3.17}$$

We see that it is possible to write both electron densities as

$$\langle n_{i\sigma}\rangle = \frac{\langle n_{i\uparrow}\rangle + \langle n_{i\downarrow}\rangle}{2} = \frac{\langle n_i\rangle}{2}, \tag{3.18}$$

where, of course, $\langle n_i\rangle$ is the summation of both electron densities with spin up and down. Using the previous statement about the symmetry of solutions (u, v) and ($-v^*$, u^*), we can write $\langle n_i\rangle$ as

$$\begin{aligned}\langle n_i\rangle = 2\langle n_{i\uparrow}\rangle &= 2\sum_n{}'[|u_i^n|^2 f(E_n) + |v_i^n|^2(1-f(E_n))]\\ &= 2\sum_n{}'|v_i^n|^2 f(-E_n).\end{aligned} \tag{3.19}$$

The last three terms in equation 3.5 makes a new term appears in the new Hamiltonian. By inserting them together with operator number and using equation 3.18 we obtain (dropping constant terms, that is, with no operators along):

$$\begin{aligned}&\sum_{i,\sigma}(V_i-\mu)n_{i,\sigma} + \sum_i(|U|\langle n_{i\uparrow}\rangle n_{i\downarrow} + |U|\langle n_{i\downarrow}\rangle n_{i\uparrow})\\ =&\sum_{i,\sigma}(V_i-\mu)n_{i,\sigma} - \sum_i\left(|U|\frac{\langle n_i\rangle}{2}n_{i\downarrow} + |U|\frac{\langle n_i\rangle}{2}n_{i\uparrow}\right)\\ =&\sum_i(V_i-\mu)n_{i,\sigma} - \frac{|U|}{2}\sum_{i,\sigma}\langle n_i\rangle\,(n_{i\downarrow}+n_{i\uparrow})\\ =&\sum_i\left[(V_i-\mu)n_{i,\sigma} - \frac{|U|}{2}\langle n_i\rangle n_{i,\sigma}\right]\end{aligned} \tag{3.20}$$

Thus, $h_{ij,\sigma}$ can be written by collecting the operators which connects single particle states:

$$\sum_{ij\sigma}c_{i\sigma}^\dagger h_{ij,\sigma}c_{i\sigma} = -t\sum_{\langle ij\rangle,\sigma}(c_{i\sigma}^\dagger c_{j\sigma} + H.c.) + \sum_i(V_i-\tilde{\mu}_i)n_{i\sigma} \tag{3.21}$$

here, $\tilde{\mu}_i$ is the new chemical potential that incorporates the site-dependent Hartree shift and it can be written in terms of the remaining terms:

$$\tilde{\mu}_i = \mu + |U|\langle n_i \rangle/2. \tag{3.22}$$

The mean field Hamiltonian can be written as

$$H_{MF} = -t \sum_{\langle ij \rangle, \sigma} (c^\dagger_{i\sigma} c_{j\sigma} + H.c.) + \sum_i (V_i - \tilde{\mu}_i) n_{i\sigma} + \sum_i [\Delta_i c^\dagger_{i\uparrow} c^\dagger_{i\downarrow} + \Delta^*_i c_{i\uparrow} c_{i\downarrow}], \tag{3.23}$$

generates the equations to be solved:

$$\begin{aligned} E_n u^n_i &= \sum_j h_{ij,\uparrow} u^n_j + \Delta_i v^n_i, \\ E_n v^n_i &= -\sum_j h^*_{ij,\downarrow} v^n_j + \Delta^*_i u^n_i, \end{aligned} \tag{3.24}$$

with the self-consistent conditions

$$\Delta_i = g \sum_n{}' u^n_i v^{n*}_i \tanh\left(\frac{E_n}{2k_B T}\right), \tag{3.25}$$

$$\langle n_i \rangle = \sum_n{}' |v^n_i|^2 f(-E_n). \tag{3.26}$$

Yet, we have:

$$h_{ij,\sigma} = -t(\delta_{i,j+\widehat{x}} + \delta_{i,j-\widehat{x}} + \delta_{i,j+\widehat{y}} + \delta_{i,j-\widehat{y}}) + (V_i - \tilde{\mu}_i)\delta_{i,j} \tag{3.27}$$

Mathematically, the Hartree shift arises from the presence of a mean-field potential term in the BdG equations, which couples the quasiparticles to the average density of the condensate. This potential term effectively accounts for the repulsion between quasiparticles caused by their interaction with the condensate. The Hartree shift modifies the energy spectrum of the quasiparticles, shifting it by an amount proportional to the average density of the condensate.

The Hartree shift is important because it affects the properties and excitations of the system. It can lead to a renormalization of the quasiparticle energies and affect transport properties, thermodynamic properties, and other observables. In some cases, it may also lead to the formation of collective modes, such as plasmons or Bogoliubov-Anderson modes, which are associated with the oscillations of the condensate density.

The order parameter Δ_i is a sum of terms of form $u_n v^*_n$. Such terms are only nonzero on the neighborhood of the Fermi surface, then it is a strong function of the temperature. In case of bulk clean materials, Δ_i is constant. When Δ_i varies spatially due to disorder, for instance, it is more difficult to ensure the convergence of the self-consistent equations. (GENNES, 1999)

3.4 CHEBYSHEV BDG METHOD

The Chebyshev-BdG method is a numerical technique used to solve the Bogoliubov-de Gennes (BdG) equations, which describe the behavior of quasiparticles in superconducting. It combines the BdG equations with the Chebyshev polynomial expansion to efficiently and accurately compute the quasiparticle spectrum and wavefunctions.

The Chebyshev-BdG method leverages the properties of Chebyshev polynomials, which are a set of orthogonal polynomials defined on a finite interval. These polynomials have advantageous properties for numerical calculations, such as the ability to efficiently approximate functions and the availability of fast algorithms for polynomial evaluation.

The Chebyshev-BdG method has several advantages. It is particularly well-suited for systems with a large number of quasiparticle states, as it provides an efficient way to compute the entire spectrum. The method can also handle spatial inhomogeneity and disorder, allowing for the study of realistic systems. Additionally, it can be extended to include finite temperature effects, making it applicable to a wide range of physical situations (NAGAI; OTA; MACHIDA, 2012).

3.4.1 The Hamiltonian

In this section, we begin by discussing the Hamiltonian associated with the BdG Equations, where Covaci (COVACI; PEETERS; BERCIU, 2010) proposed an alternative approach that avoids full diagonalization.

Consider a Hamiltonian for a fermionic system given by $H = \frac{1}{2}\Psi^{\dagger}\mathcal{H}\Psi$. Here, the column vector Ψ is constructed from N fermionic annihilation and creation operators, denoted as c_i and $c_i^{\dagger}$ respectively, where $i = 1, 2, ..., N$. Thus, we can express Ψ as $(c_i, c_i^{\dagger})^T$. The fermionic canonical anti-commutation relation is given by $[c_i, c_j^{\dagger}]+ = \delta_{ij}$.

The "Hamiltonian" matrix $\mathcal{H}$ is a Hermitian matrix of size 2Nx2N, defined as:

$$\mathcal{H} = \begin{pmatrix} \widehat{A} & \widehat{B} \\ \widehat{B}^{\dagger} & -\widehat{A}^{\dagger} \end{pmatrix}. \tag{3.28}$$

Here, $\widehat{A}$ and $\widehat{B}$ are complex N x N matrices that satisfy the relations:

$$\widehat{A}^{\dagger} = \widehat{A}, \quad \widehat{B}^{T} = -\widehat{B}. \tag{3.29}$$

When considering a superconductor, the matrix $\mathcal{H}$ corresponds to the mean-field BCS Hamiltonian, while $\widehat{B}$ represents the superconducting gap.

3.4.2 BdG Equation

The following eigen-problem is known as the BdG Equations expressed in terms of $\mathcal{H}$

$$\mathcal{H}\mathbf{f}_\gamma = \epsilon_\gamma \mathbf{f}_\gamma, \tag{3.30}$$

where

$$\mathbf{f}_\gamma = \begin{pmatrix} \mathbf{u}_\gamma \\ \mathbf{v}_\gamma \end{pmatrix}. \tag{3.31}$$

the column vectors $\mathbf{u}_\gamma$ and $\mathbf{v}_\gamma$ are N-component complex vectors. The solution to the BdG Equation is equivalent to diagonalization of $\mathcal{H}$ with a unitary matrix $\widehat{U}$,

$$\widehat{U}^\dagger \mathcal{H} \widehat{U} = \widehat{D}, \quad \widehat{D} = diag(\epsilon_1, \epsilon_2, ..., \epsilon_{2N}). \tag{3.32}$$

Of course, the matrix elements of $\widehat{U}$ are

$$U_{i\gamma} = u_{\gamma,i}, \quad U_{i+N,\gamma} = v_{\gamma,i}. \tag{3.33}$$

3.4.3 Spectral Density

The spectral density $\widehat{d}(\omega)$ is a 2N x 2N matrix that encompasses essential physical observables expressed as bilinear forms with respect to $\widehat{d}(\omega)$.

Let's define the Green's function as $\widehat{G}(z) = (z - \widehat{H})^{-1}$. Using the unitary matrix $\widehat{U}$, each component of $\widehat{G}(z)$ can be expressed as:

$$G_{\alpha\beta} = \sum_{\gamma=1}^{2N} U_{\alpha\gamma} U^*_{\beta\gamma} \frac{1}{z - \epsilon_\gamma}, \tag{3.34}$$

where $(1 \leq \alpha, \beta \leq 2N)$. By setting $z = i\omega_n$ with the Matsubara frequency $\omega_n = (2n+1)/\beta$, the equation above becomes the temperature Green's function. The retarded and advanced Green's functions are defined as:

$$\widehat{G}^R(\omega) = \lim_{\eta \to 0+} \widehat{G}(\omega + i\eta), \tag{3.35a}$$

$$\widehat{G}^A(\omega) = \lim_{\eta \to 0+} \widehat{G}(\omega - i\eta), \tag{3.35b}$$

The spectral density is given by the difference between the advanced and retarded Green's functions, $\widehat{d}(\omega) \equiv \widehat{G}^R(\omega) - \widehat{G}^A(\omega)$, and its matrix elements are expressed as:

$$d_{\alpha\beta}(\omega) = -2\pi i \sum_{\gamma=1}^{2N} U_{\alpha\gamma} U^*_{\beta\gamma} \delta(\omega - \epsilon_\gamma). \tag{3.36}$$

To obtain physical observables from $\widehat{d}(\omega)$, we introduce the following useful 2N-component unit vectors $\mathbf{e}(i)$ and $\mathbf{h}(i)$ $(1 \leq i \leq N)$, defined as:

$$[\mathbf{e}(i)]_\gamma = \delta_{i,\gamma}, \quad [\mathbf{h}(i)]_\gamma = \delta_{i+N,\gamma}. \tag{3.37}$$

Using the notation above, we can express the column vectors $\mathbf{u}\gamma$ and $\mathbf{v}\gamma$ as:

$$\mathbf{u}_{\gamma,i} = [\mathbf{e}(i)^T \widehat{U}]_\gamma, \tag{3.38a}$$

$$\mathbf{v}^*_{\gamma,i} = [\widehat{U}^\dagger \mathbf{h}(i)]_\gamma. \tag{3.38b}$$

A typical self-consistent BdG calculation for a superconductor requires two types of mean-fields, $\langle c_i^\dagger c_j \rangle$ and $\langle c_i c_j \rangle$. These mean-fields can be expressed as:

$$\langle c_i^\dagger c_j \rangle = -\frac{1}{2\pi i} \int_{-\infty}^{\infty} d\omega f(\omega) \mathbf{e}(j)^T \widehat{d}(\omega) \mathbf{e}(i), \tag{3.39a}$$

$$\langle c_i c_j \rangle = -\frac{1}{2\pi i} \int_{-\infty}^{\infty} d\omega f(\omega) \mathbf{e}(j)^T \widehat{d}(\omega) \mathbf{h}(i), \tag{3.39b}$$

where $f(x) = 1/(e^{\beta x} + 1)$ and β is the inverse temperature. The Chebyshev method aims to expand the spectral density $\widehat{d}(\omega)$ in terms of Chebyshev polynomials for improved numerical efficiency.

3.4.4 Orthogonal Polynomials

In a typical mathematical physics course, we learn about the expansion of functions in terms of orthogonal polynomials within a specific interval. In the context of solving BdG equations, various orthogonal polynomials are employed. These polynomials satisfy the relation:

$$\delta(x - x') = \sum_{n=0}^{\infty} \frac{W(x)}{w_n} \phi_n(x) \phi_n(x'), \tag{3.40}$$

where the weight function $W(x)$ and the coefficients w_n are given by:

$$w_n \delta_{n,m} = \int_{-1}^{1} \phi_n(x) \phi_m(x) W(x) dx. \tag{3.41}$$

The recurrence formula for these orthogonal polynomials is commonly expressed as (HASSANI, 2013):

$$\phi_{n+1} = (a_n + b_n x)\phi_n(x) - c_n\phi_{n-1}(x). \tag{3.42}$$

To ensure that the eigenvalues lie within the convergence interval, the energy of $\mathcal{H}$ is rescaled as follows:

$$\mathcal{K} = \frac{\mathcal{H} - bI}{a}, \quad \xi_\gamma = \frac{\epsilon_\gamma - b}{a}, \tag{3.43}$$

where $a = (E_{\text{max}} - E_{\text{min}})/2$ and $b = (E_{\text{max}} + E_{\text{min}})/2$, with $E_{\text{min}} \leq \epsilon_\gamma \leq E_{\text{max}}$. The values of a and b can be approximately estimated to satisfy the rescaling condition, as significant changes in the rescale do not significantly affect the results - as shown in reference (TANAKA; KUNISHIMA; ITOH, 2000). By defining a matrix using the polynomial function, we have:

$$[\phi_n(\mathcal{K})]_{\alpha\beta} = \sum_{\gamma=1}^{2N} U_{\alpha\gamma}U^*_{\beta\gamma}\phi_n(\xi_\gamma), \tag{3.44}$$

where $\phi_n(\xi_\gamma)$ is well-defined within the interval $\xi_\gamma \in [-1, 1]$. The integrals over ω in Eq. 3.39 are also bounded within a finite energy range. Substituting the right-hand side of Eq. 3.40 into the definition of $\widehat{d}(\omega)$, we obtain:

$$\mathbf{p}^T\widehat{d}(\omega)\mathbf{q} = -\frac{2\pi i}{a}\sum_{n=0}^{\infty}\frac{W(\omega)}{w_n}\phi_n(\omega)\mathbf{p}^T\mathbf{q}, \tag{3.45}$$

for arbitrary 2N-component real vectors $\mathbf{p}$ and $\mathbf{q}$. A sequence of vectors $\mathbf{q}n = \phi_n(\mathcal{K}\mathbf{q})$ is recursively generated by:

$$\mathbf{q}_{n+1} = (a_n + b_n\mathcal{K})\mathbf{q}_n - c_n\mathbf{q}_{n-1}, \tag{3.46a}$$

$$\mathbf{q}_1 = \phi_1(\mathcal{K})\mathbf{q}, \tag{3.46b}$$

$$\mathbf{q}_0 = \phi_0(\mathcal{K})\mathbf{q}. \tag{3.46c}$$

The coefficients in Eq. 3.46a are the same as in Eq. 3.42. The mean fields can then be written as:

$$\langle c_i^\dagger c_j\rangle = \sum_{n=0}^{\infty}\mathbf{e}(j)^T\mathbf{e}_n(i)\frac{\mathcal{T}_n}{w_n}, \tag{3.47a}$$

$$\langle c_i c_j\rangle = \sum_{n=0}^{\infty}\mathbf{e}(j)^T\mathbf{h}_n(i)\frac{\mathcal{T}_n}{w_n}, \tag{3.47b}$$

where

$$\mathcal{T}_n = \int_{-1}^{1} dx f(ax+b)W(x)\phi_n(x) \tag{3.48}$$

and

$$\mathbf{e}_n(i) = \phi_n(\mathcal{K})\mathbf{e}(i), \quad \mathbf{h}(i) = \phi_n(\mathcal{K})\mathbf{h}(i) \tag{3.49}$$

In the following sections, we utilize Chebyshev polynomials given by:

$$\phi_n(x) = \cos\left(n \arccos\left(x\right)\right), \tag{3.50}$$

$$W(x) = \frac{1}{\sqrt{1-x^2}}, \quad w_n = \frac{\pi}{2}(1+\delta_{n0}), \quad x = [-1,1]. \tag{3.51}$$

The coefficients in the recursive formula are $a_n = 0$, $b_n = 2$, and $c_n = 1$. The vector form of the formula associated with equation 3.46a is given by:

$$\mathbf{q}_{n+1} = 2\mathcal{H}\mathbf{q}_n - \mathbf{q}_{n-1}, \quad (n \geq 2) \tag{3.52}$$

with $\mathbf{q}_0 = \mathbf{q}$ and $\mathbf{q}_1 = \mathcal{K}\mathbf{q}$. Throughout this thesis, all the cases studied in the main work are at zero temperature. Therefore, a few integrals can be solved analytically, leading to the following results:

$$\mathcal{T}_0 = \pi - \arccos\left(-b/a\right), \tag{3.53a}$$

$$\mathcal{T}_{n\neq 0} = -\frac{\sin\left[n \arccos\left(-b/a\right)\right]}{n}. \tag{3.53b}$$

Furthermore, the utilization of Chebyshev polynomials in the Chebyshev-BdG method is motivated by their rapid convergence properties. This allows for convergence with a relatively small number of terms, thereby facilitating the truncation of the summation process. For instance, it has been observed that truncating the summation at approximately 2000 terms in equation 3.47 is generally sufficient to achieve good convergence. It is important to note, however, that more exotic cases may require separate analysis and consideration since more ou less terms in Chebyshev expantion may be required in order to obtain good convergence. Someone who is willing to test is suggested to start with a small number of terms (500, for instance) and perform several trials increasing the number of terms until results do not differ from the previous trial.

4 DISORDER IN SUPERCONDUCTORS

Disorder plays a significant role in the behavior of superconducting systems. In the context of superconductivity, disorder refers to imperfections, impurities, or random variations in the crystal lattice or other aspects of the material. These disorder-induced effects can have profound consequences on the superconducting properties, including the critical temperature, coherence length, and quasiparticle dynamics.

Figure 7 – Two crystalline lattices are represented. They are an example of what disorder means in our context: Displacements of atoms from their equilibrium position. Left: Representation of a ordered crystalline lattice. Right: Representation of a disordered crystalline lattice.

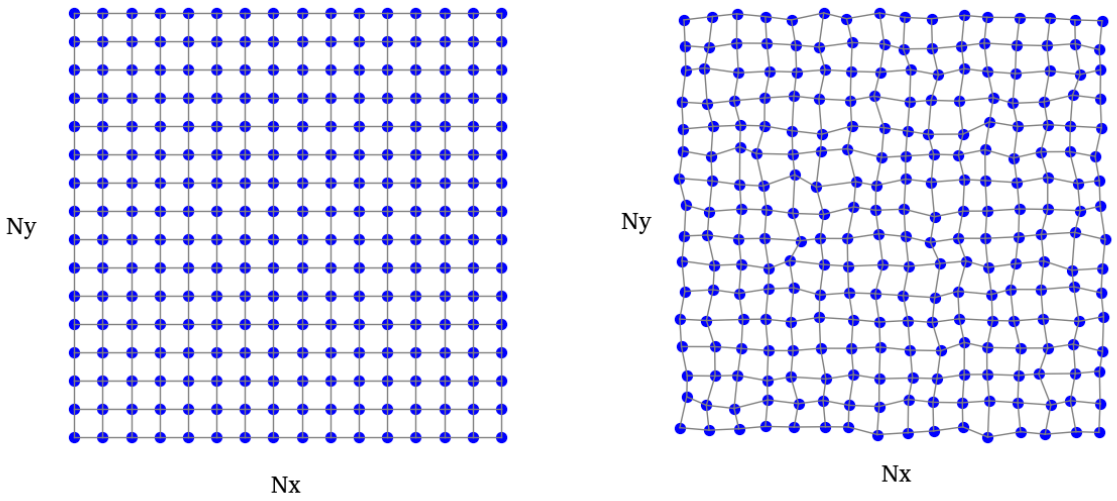

Source: The Author (2023).

One of the key effects of disorder in superconductivity is the suppression of the critical temperature (T_c) when the disorder is strong enough. For weak disorder we have to talk about Anderson Theorem which will be done later, in the next section. In clean or pristine superconductors, T_c represents the temperature below which the material undergoes a transition to the superconducting state. However, the presence of disorder scatters the electrons and disrupts the formation of Cooper pairs, leading to a reduction in T_c. This effect is commonly known as Anderson localization, named after physicist P. W. Anderson, who first described it.

Disorder can also induce inhomogeneities or spatial variations in the superconducting order parameter. This can lead to the formation of localized regions of superconductivity, known as superconducting islands or puddles, embedded within a background of normal or

non-superconducting regions. Such spatial variations are particularly relevant in thin films or nanoscale superconducting structures, where disorder can play a dominant role.

Understanding and characterizing the effects of disorder in superconductivity is crucial for various applications. Disorder can limit the performance of superconducting devices, such as Josephson junctions or superconducting qubits used in quantum computing. On the other hand, disorder can be intentionally introduced to engineer novel phenomena, such as the emergence of topological superconductivity or the formation of Majorana bound states.

4.1 ANDERSON THEOREM FOR DISORDERED SUPERCONDUCTORS

In conventional s-wave superconductors, disorder has very little effect on the superconducting transition temperature and other physical quantities. This phenomena was first noticed by Anderson. He gave an explanation of this phonemona based on the self-consistent mean-field theory (ANDERSON, 1959), it is oftenly refered as Anderson Theorem. It is valid only for weak disorder, when the time reversal is preserved and when the order parameter is homogeneous (XIANG; WU, 2022).

Two approximations are taken into account in the proof of the Anderson Theorem. First, the variation of the order parameter $\Delta(\mathbf{r})$ is said to be small so that it can be replaced by its average value, $\Delta(\mathbf{r}) = \Delta$. This approximation implies that the self-consistent mean-field equation of the gap energy is just a result of the spatial averaging. Second, the scattering potential does not change the density of states around the Fermi surface of normal electrons. These two approximations are generally valid if the disorder scattering potential is not very strong. But the first approximation holds only when the correlation length is much larger than the scattering mean free path. Under these approximations, the BdG equation in its continuum version is given by:

$$\begin{aligned} E_n u^n(\mathbf{r}) &= \int d\mathbf{r}' h(\mathbf{r}, \mathbf{r}') u^n(\mathbf{r}') + \Delta v^n(\mathbf{r}), \\ E_n v^n(\mathbf{r}) &= -\int d\mathbf{r}' h^*(\mathbf{r}, \mathbf{r}') v^n(\mathbf{r}') + \Delta u^n(\mathbf{r}), \end{aligned} \tag{4.1}$$

where we use the free electron gas Hamiltonian

$$h(\mathbf{r}, \mathbf{r}') = \delta(\mathbf{r} - \mathbf{r}') \left(-\frac{\hbar^2}{2m} \nabla^2 + U(\mathbf{r}) - \mu \right), \tag{4.2}$$

where $U(\mathbf{r})$ is the impurity scattering potential.

The order parameter Δ does not depends on $\mathbf{r}$. If $w_n(\mathbf{r})$ is the eigenstate of normal electrons

$$\int d\mathbf{r}' h(\mathbf{r},\mathbf{r}')w_n(\mathbf{r}') = \xi_n w_n(\mathbf{r}), \tag{4.3}$$

we can propose the following ansatz for u and v

$$u_n(\mathbf{r}) = u_n w_n(\mathbf{r}), \quad v_n(\mathbf{r}) = v_n w_n(\mathbf{r}). \tag{4.4}$$

Substituting in the BdG Equation in continuum we obtain a simplified equation

$$\begin{aligned} \xi_n u_n + \Delta v_n &= E_n u_n, \\ \Delta u_n - \xi_n v_n &= E_n v_n, \end{aligned} \tag{4.5}$$

with this we generate an eigenproblem which can be easily solved as a 2x2 matrix determinant. It has exactly the same form as the standard BCS mean-field equation for a translation invariant system. The difference is that now the momentum is not a good quantum number since it is not conserved. Instead, the basis states are characterized by the quantum number n of $h(\mathbf{r},\mathbf{r}')$. The diagonalization of the previous equation provides us the quasiparticle eigenenergy

$$E_n = \sqrt{\xi_n^2 + \Delta^2} \tag{4.6}$$

and the corresponding eigenfunction

$$u_n = \sqrt{\frac{1}{2}\left(1 + \frac{\xi_n}{E_n}\right)}, \quad v_n = -\sqrt{\frac{1}{2}\left(1 - \frac{\xi_n}{E_n}\right)}. \tag{4.7}$$

The order parameter can be determined by the usual equation

$$\Delta = -g\sum_n u_n(\mathbf{r})v_n(\mathbf{r})\tanh\frac{\beta E_n}{2}. \tag{4.8}$$

Substituting the solutions for u and v in the equation for the order parameter, we obtain

$$\begin{aligned} \Delta &= g\sum_n \langle w_n^2(\mathbf{r})\rangle \frac{\Delta}{2\sqrt{\xi_n^2+\Delta^2}} \tanh\frac{\beta\sqrt{\xi_n^2+\Delta^2}}{2} \\ &= g\int d\xi N(\omega)\frac{\Delta}{2\sqrt{\xi^2+\Delta^2}} \tanh\frac{\beta\sqrt{\xi^2+\Delta^2}}{2}, \end{aligned} \tag{4.9}$$

where here $N(\omega)$ is the normal-state single-particle density of states for disordered systems

$$N(\xi) = \sum_n \delta(\xi - \xi_n)\langle w_n^2(\mathbf{r})\rangle \tag{4.10}$$

and $\langle w_n^2(\mathbf{r})\rangle$ is the spacial average of w_n^2.

Since the impurity scattering does not change the density of states of normal electrons around the Fermi surface according to the previous assumption, the order parameter equation seen in 4.9 has exactly the same form as the gap equation for the impurity-free system with $U(\mathbf{r}) = 0$. Thus the impurity scattering does not change the transition temperature T_c of the s-wave superconductor. This is the proof first given by Anderson. It is consistent with experimental observations for conventional superconductors.

4.2 STRONG DISORDER EFFECTS

Disorder in low dimensional superconductors have hot a boost from experiments in superconducting films, which have shown that transition temperature changes as disorder increases and leads to a new phenomena not predicted by Anderson Theorem. The physics of high disordered films is outside the domain of Anderson Theorem. The effect of strong disorder in superconductors is a challenge in theoretical condensed matter physics. Using the BdG approach, not only is necessary to assume the spatial variation on the order parameter Δ_i, that is, its spatial inhomogeneties. In special, as we increase disorder by solving BdG Equations it is possible to see how the order parameter changes by plotting a histogram of all possible values for Δ_i given a certain disorder. The disorder used commonly is given by an impurity potential defined by an independent random variable V_i uniformly distributed over $[-V, V]$, at each site in the sample. V is this case controls the strength of the disorder.

Ghosal showed on his work (GHOSAL; RANDERIA; TRIVEDI, 2001) that as we increase disorder the statistics of the order parameter and the average local density of electrons change. Solving the BdG equations for samples with periodic boundary condition with size 24 x 24 and performing 15 random samples it is possible to generate the Figure 8, which shows the Histograms of the local order parameter for several disordered samples with size 24 x 24, $\langle n \rangle$ = 0.875 and U = -1.5t.

When V = 0, the BdG solution returns the uniform order parameter $\Delta_0 = 0.153t$. For V = 0.1t, the distribution has a sharp peak about Δ_0, which resembles a lot that is expected from Anderson theorem. Increasing more the disorder, from $V \approx 1t$ on, $P(\Delta)$ becomes broad and the assumption of a uniform Δ breaks down. For values larger than V = 2t the disorder has most values close to $\Delta_i = 0$. Contrasting the previous results with the distribution of the local density P(n), still have a peak for weak disorder around the value $\langle n \rangle = 0.875$, but as we increase disorder it evolves to an almost bimodal distribution for large V, with sites being

Figure 8 – Histogram of order parameter for several disorder values

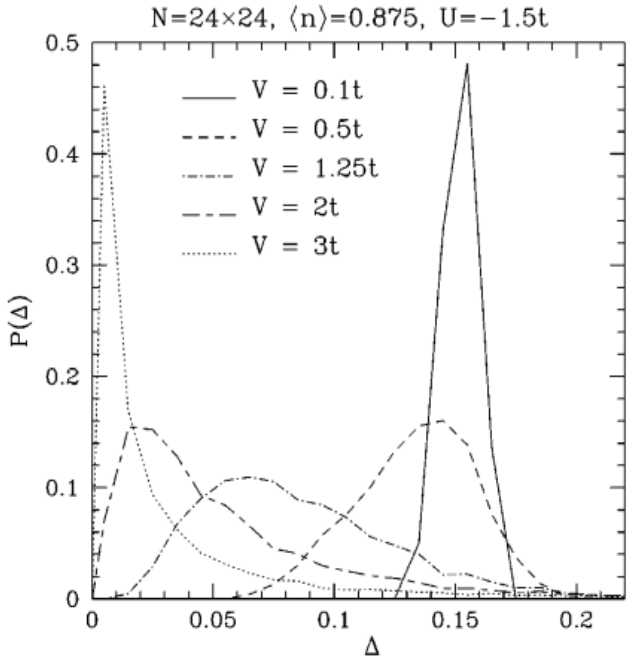

Source: Ghosal, Randeria and Travedi (2001)

empty or filled.

The local distribution of the order parameter is illustrated in Figure 9. It demonstrates that as the disorder is increased, superconducting islands begin to emerge within the material. These islands represent localized regions where superconductivity is present, separated by regions with very small Δ_i values. By analyzing the correlation between the island locations and the underlying random potential across multiple realizations, it is observed that large Δ_i values tend to occur in regions where $|V_i - \tilde{\mu}_i|$ is small, facilitating significant particle-hole mixing. Conversely, deep valleys and high mountains in the potential energy landscape correspond to sites with a fixed number of particles: two on a valley site or zero on a mountain site. Consequently, the local pairing amplitude vanishes in such regions. The grey regions in the figure represent the superconducting islands, where superconductivity is still present. It is evident that as disorder increases, it becomes reasonable for P(Δ) to approach zero. Despite the low average order parameter of the system, localized pockets of superconductivity persist throughout the material.

Figure 9 – Histogram of local electron density for several disorder values.

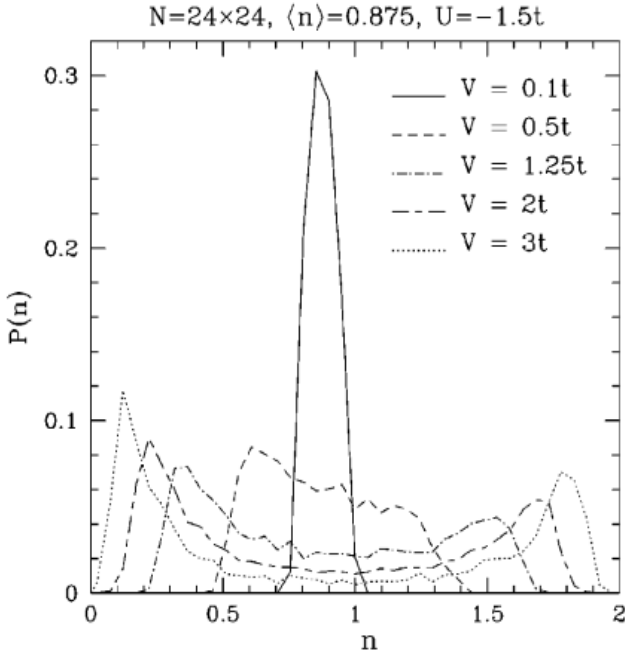

Source: Ghosal, Randeria and Trivedi (2001).

Figure 10 – Appearance of superconducting islands with increasing disorder. The figure shows four different samples with the disorder strength (V) varying from t to 3t. The darker areas are the regions where the order parameter is non-zero, while white areas are where order parameters are zero.

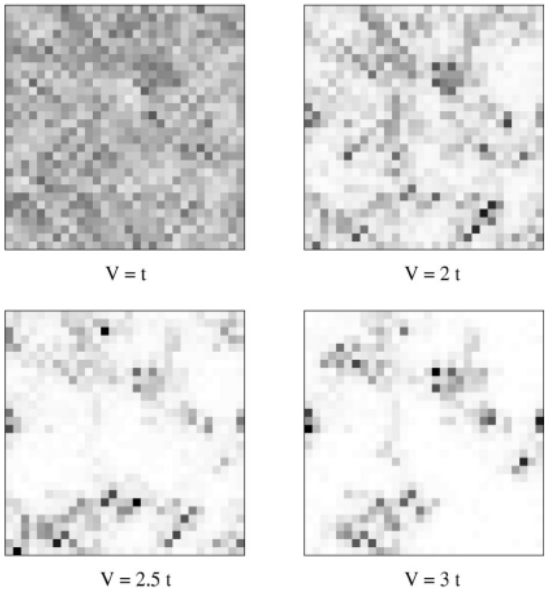

Source: Ghosal, Randeria and Travedi (2001)

4.3 CORRELATED DISORDER

Correlated disorder, also known as correlated randomness or correlated disorder phenomena, refers to a type of disorder where the elements or components of a system exhibit some form of non-random behavior despite being disordered as a whole. In such systems, although the individual elements may not be arranged in an ordered or predictable manner, there are correlations or dependencies between them that give rise to emergent patterns or collective behaviors (FEDER, 1988).

Correlated disorder can be observed in various natural and artificial systems across different scientific domains, including physics, biology, and social sciences. It often arises from complex interactions between individual components, leading to interesting and sometimes unexpected macroscopic phenomena. Here are a few examples (MANDELBROT, 1982):

- Spin Glasses: In condensed matter physics, spin glasses are materials composed of magnetic atoms with randomly oriented spins. Although the spins individually behave randomly, their interactions lead to complex collective behavior characterized by the existence of "frustrated" states and slow relaxation dynamics.

- Biological Systems: Correlated disorder can also be found in biological systems. For instance, in neural networks, the firing patterns of individual neurons may be stochastic, yet their collective behavior gives rise to coordinated activity and information processing. Genetic regulatory networks, protein folding, and ecological systems are other examples where correlated disorder plays a role.

- Financial Markets: In economics and finance, correlated disorder is observed in the behavior of financial markets. While the movements of individual stocks may appear random, there are often correlations or dependencies between their price fluctuations. These correlations can arise from various factors, such as market sentiment, news events, or underlying economic fundamentals.

- Social Networks: In the realm of social sciences, social networks exhibit correlated disorder. While individual interactions within a network may be random or unpredictable, there are often patterns of clustering, community formation, and information propagation that emerge from the collective behavior of networked individuals.

Understanding and characterizing correlated disorder is a challenging task, as it involves deciphering the intricate relationships and interactions between the elements of a system. Statistical physics, network theory, and computational modeling are among the tools used to study and analyze such systems. By unraveling the underlying mechanisms that give rise to correlated disorder, scientists aim to gain insights into the complex dynamics and emergent properties of various natural and artificial systems.

Several stochastic processes in nature are known to generate long-range correlated random sequences which have no characteristic scale. These sequences usually have an approximate powerlaw spectral density of the form

$$S(q) \propto 1/q^{\alpha} \tag{4.11}$$

where $S(q)$ is the Fourier transform of the two-point correlation function $\langle V_i V_j \rangle$. The power exponent α determines the correlation degree. When $\alpha = 0$ the random potential V_i at different lattice sites is fully uncorrelated. The widespread occurrence in nature of sequences with $1/q^{\alpha}$ noise, as, for example, the nucleotide sequency in DNA molecules, seems to be related to the general tendency of large driven dynamical systems to evolve for a self-organized critical state.

Inspired on works of Fidelis (MOURA; LYRA, 1998) and Neverov (NEVEROV et al., 2022) who studied correlated disorder on solids, in this dissertation we generate correlated random numbers where the correlations can occur in x and y directions to mimic the disordered potential on solid. The correlated disorder used here is given by the formula

$$V_i = \frac{1}{N^2} \sum_{j_x, j_y}^{N_x/2, N_y/2} q_j^{-\alpha/2} \cos\left(\mathbf{q}_j \mathbf{r}_i + \phi_j\right), \tag{4.12}$$

where $\mathbf{r}_i$ is the lattice position and $\mathbf{q}_j = (2\pi j_x/N_x, 2\pi j_y/N_y)$ is the discrete inverse space vector, $j_{x,y} = 1, 2, ..., N_x$ or N_y. The phases ϕ_i are random numbers distributed within $[0, 2\pi)$. In order to tame the strength and average value, it is interesting to shift the potential as

$$V_i \to V_i - \overline{V_i}, \quad \overline{V_i} = \sum_i \langle V_i \rangle. \tag{4.13}$$

The disorder amplitude, or strenth, is defined by the quantity

$$V = \sqrt{\overline{V_i^2}}, \tag{4.14}$$

that is, the standard deviation (NEVEROV et al., 2022).

4.4 EFFECTS OF CORRELATED DISORDER ON SUPERCONDUCTIVITY

Most theoretical investigations of disordered superconductors are based on the models with the spatially uncorrelated disorder, which are analyzed using the perturbation expansion methods. In real systems, however, the disorder is almost never completely random. The inhomogeneities are often arranged in a certain structure, characterized by the long-range spatial correlations. Very little is known about inherently random distribution of material inhomogeneities acquires a certain degree of spatial correlations.

On Neverov's work (NEVEROV et al., 2022), it is shown how correlation affects the statistics of order parameter by solving the BdG Equation with periodic boundary condition and size 40 x 40. The correlation degree is usually changed from 0 to 3 for several different disorder strength. The number of statistical samplings are 40. The following images show the plots of superconducting islands with increasing α and V and its statistics.

In figure 4.4, we see how superconducting islands changes as we increase correlations in the random potential. Superconducting islands tend to get bigger as we increase disorder strength. The blue color indicates domains of the superconductive phase of order parameter different of zero and the white color marks domains of the normal phase with order parameter close to zero.

The distribution of the order parameter resembles Ghosal's results for $\alpha = 0$, but it changes dramatically in case of $V = 2.0t$. In fact, even for small disorder we see the effect of correlations: the change in the average value away from zero. As expected, it gets more likely to have $\Delta_i \approx 0$ as we increase disorder, but they tends to be tamed as we increase correlations. It is visible that the distribution changes dramatically in $V = 2.0t$ from $\alpha = 2$ on. These changes can be seen also by analysing the standard deviation σ and the maximum $\Delta_{max}/\overline{\Delta}$. This analysis of the order parameter distribution and its defining characteristics quantify visual changes seen in the order parameter profile in Figure 4.4.

Figure 11 – Appearance of superconduting islands in superconducing sample with increasing disorder and correlation in the random potential. Row (a) shows the evolution of the disorder potential as the correlation increases. Rows (b) - (e) shows the local order parameter evolves with increasing disorder and correlation degree. The white areas is where the order parameter is zero whereas blue areas indicate non-zero order parameter. In this figure since t = 1, the disorder strength V has only numerical values, but of course we can multiply the number for t and the disorder strength would be the same.

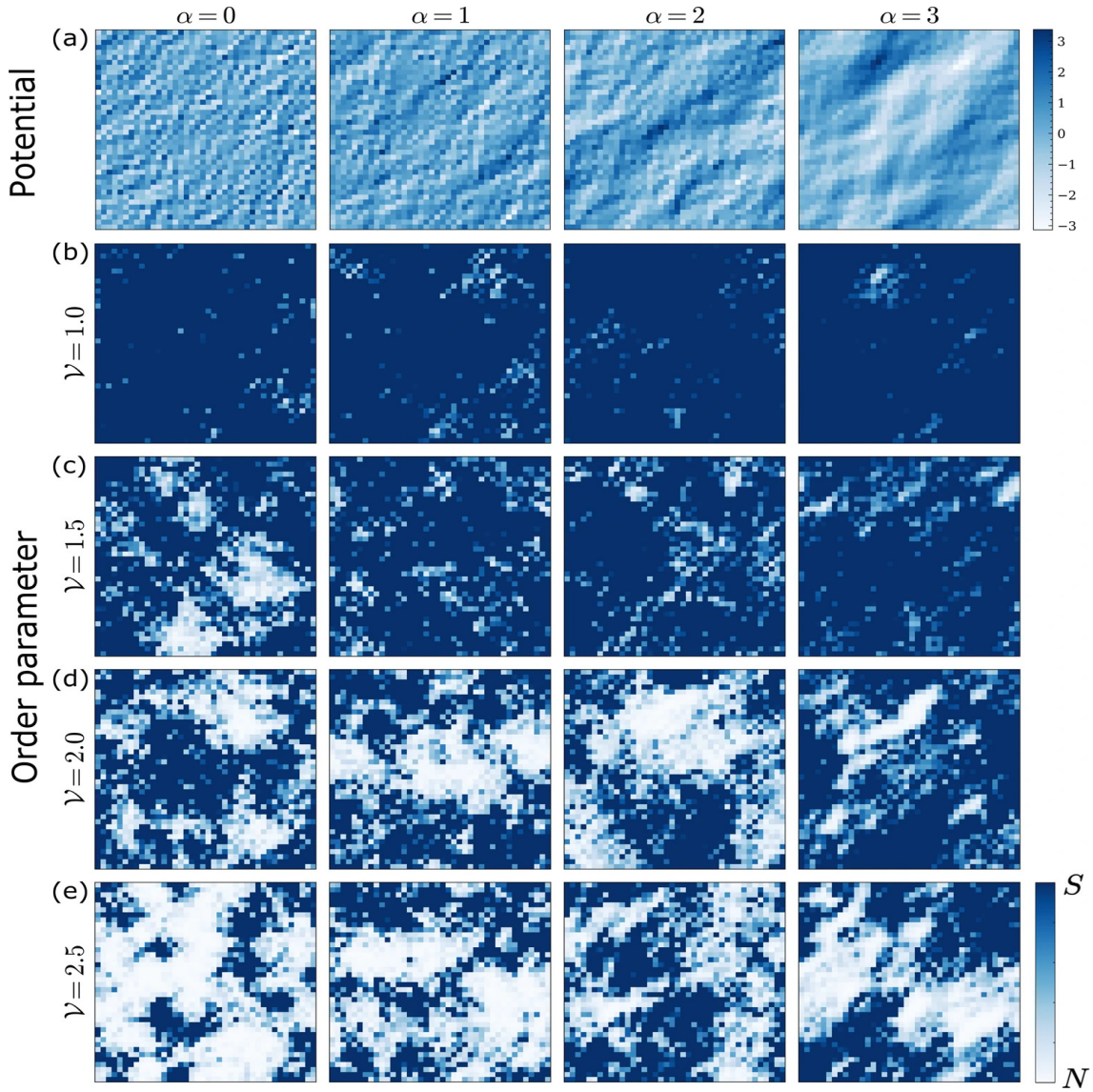

Source: Neverov et Al. (2022)

Figure 12 – Figures (a) - (c) Histogram of order Parameter for different potentials and correlations. The histogram is normalized in relation to the average order parameter $\overline{\Delta}$.

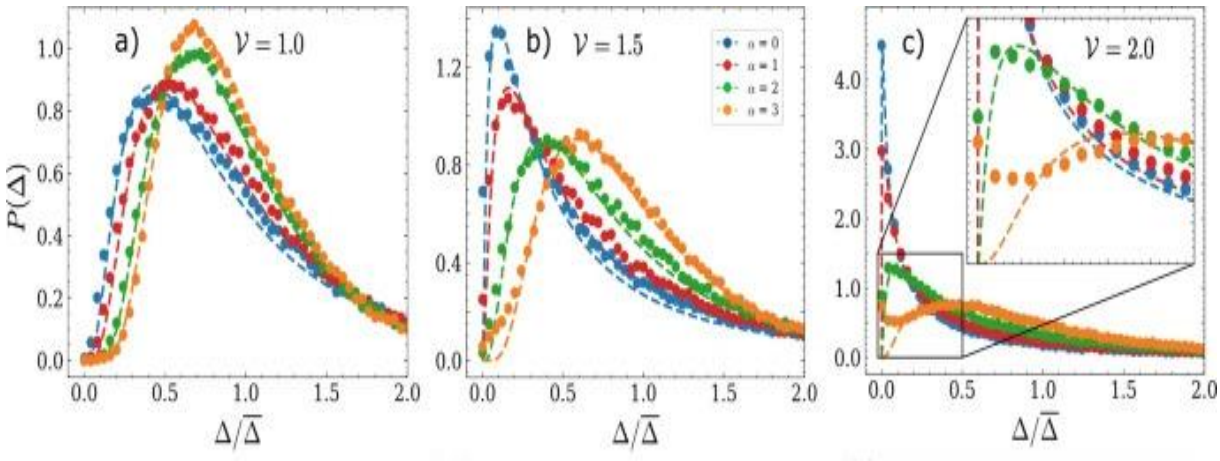

Source: Neverov et Al. (2022)

5 RESULTS AND DISCUSSION

5.1 QUANTUM OSCILATIONS IN THE ORDER PARAMETER

In recent years, significant experimental progress has sparked a strong interest in studying superconducting properties in nanostructures. These structures exhibit a unique characteristic called quantum confinement, which is discussed further. An essential aspect of this research is the ability to manipulate the size and shape of confinement, as it enhances superconductivity and leads to oscillations in the superconducting properties. Consequently, the investigation of superconductivity in nanostructures, particularly nanowires, holds fundamental importance due to the capacity to control superconducting characteristics by adjusting their cross-sectional dimensions.

Several decades ago, Blatt and Thompson conducted calculations on the energy-gap parameter of superconducting nanofilms in a clean environment, unveiling a remarkable sequence of peaks dependent on the thickness of the films (BLATT; THOMPSON, 1963). They termed these peaks as size resonances. However, at that time, producing highly crystalline superconductors with nanoscale dimensions was not feasible. Only recently have experimental observations of thickness-dependent oscillations in Tc been made in lead (Pb) nanofilms. Prior to these advancements, the interplay between quantum confinement and fermion pairing could only be experimentally studied in atomic nuclei, affirming the expectations of Blatt and Thompson through a series of size resonances in the energy gap of paired nuclei. The progress in fabricating nanosized structures holds the potential to revolutionize our understanding of the size-dependent properties of nanoscale superconductors. Notably, a study demonstrated the ability to reduce the width of nanowires to as small as 10nm using ion-beam sputtering. Additionally, recent experimental observations on clean aluminum (Al) and tin (Sn) nanowires indicate a width-dependent increase in the superconducting transition temperature, providing initial evidence of size-dependent resonances in quasi-one-dimensional superconductors (CROITORU; SHANENKO; PEETERS, 2007).

The superconducting order parameter is affected by the number of single-electron states within a specific energy range around the Fermi level, which is known as the Debye window. This parameter, represented as N_D, relies on the average energy density of these states per unit volume.

It's important to highlight that N_D provides the mean density since the density of single-

electron states can vary, especially in quasi-one-dimensional systems. In high-quality nano-films and nano-wires, where transverse quantization effects are significant and impurity scattering is minimal, the conduction band splits into multiple single-electron subbands as the thickness of the material changes. These subbands shift in energy, with the lower boundary of each subband scaling as $1/d^2$, where d refers to the thickness of the nano-film/nano-wire.

When the bottom of a parabolic subband crosses the Fermi surface, the number of contributing single-electron states suddenly increases, resulting in quantum-size oscillations in superconducting properties. This phenomenon leads to significant improvements in superconductivity, referred to as size-dependent superconducting resonances. The occurrence of these resonances follows a sequential pattern: as the thickness increases, a particular subband labeled as n enters the Debye window, causing a sharp rise in N_D and the onset of a superconducting resonance. The subsequent resonance emerges when subband $n+1$ enters the Debye window. Consequently, the mean density N_D displays a series of peaks as a function of thickness d, resulting in quantum-size oscillations of various superconducting quantities with notable resonant enhancements.

These superconducting resonances are particularly significant in nanoscale samples but become less pronounced as the thickness d increases, gradually approaching the bulk limit represented by $N(0)$:

$$N\left(0\right)=\frac{mk_F}{2\pi^2\hbar^2}. \tag{5.1}$$

Here, k_F corresponds to the three-dimensional Fermi wavevector.

The oscillations occur whenever the sample size is equal to a multiple of $\lambda_F/2$, assuming that the influence of the sample size on the Fermi energy (E_F) is negligible and the electron density remains constant in the system. The oscillations occur every time the size of the sample is equal to (if we neglect the influence of the sample size on the E_F, in case we preserve constant the electron density in the system)

$$d=\frac{\lambda_F}{2}m$$

where m is an integer.

In the Hubbard model, where the band is no longer parabolic, we have atoms whose distance from each other is given by $a=x_{j=1}-x_j$, where x represents the relative position of the j-th atom. Our assumptions for the parabolic band still works very well in Hubbard model

but here we have a discrete variation in the confinement length since we can only increase our sample increasing the amount of atoms in one direction.

When the chemical potential or Fermi energy in the system resides in the proximity of the bottom or the top of the band

$$\frac{\lambda_F}{2} \gg a, \tag{5.2}$$

therefore one oscillation (due to the quantum-size-effects) occur only when we change the size of the sample by several a. Therefore oscillations are visible.

In case the chemical potential or Fermi energy in the system resides in the middle of the band

$$\frac{\lambda_F}{2} \simeq a. \tag{5.3}$$

However we can change the sample size only by integer number of a. That means any time we change the sample size we are always in the same situation: the bottom of the band in the proximity of the chemical potential (Fermi energy) and one observes only a smooth change of the superconducting characteristics with sample size without oscillations in the properties.

Nanoscale materials like quantum wires are interesting because they have potential practical applications. In such systems, the energy level discretization due to the quantum size effects is one of the most important keys. For nanoscale superconductors the effects can be even more interesting as we will see bellow.

The BdG formalism is powerful in dealing with quantum size effects. For nanoscale superconductors, the confinement effect is described by the potential $V_c(\mathbf{r})$. For a quasi 1d-superconducting nanowire, the confinement is one dimensional. In hard wall approximation, we have

$$V_c(\mathbf{r}) = \begin{cases} 0 & \text{for } 0 \leq \mathrm{x} \leq N_x, \\ \infty & \text{otherwise.} \end{cases} \tag{5.4}$$

Of course, the x direction was arbitrarily chosen, but instead calling it x, let us call it confinement direction and confinement length the nanowire width.

Our quasi-1D nanowire can be visualized as a ribbon with periodic boundary conditions along the y-direction and confinement in the x-direction. To solve the BdG equation in the nanowire, we employ the Chebyshev method. We perform multiple iterations of the Chebyshev BdG equation solver for a clean superconductor (i.e., without disorder), while varying the confinement length for two different average electron densities: $\langle n \rangle = 0.875$ and $\langle n \rangle = 0.125$.

In all calculations, we use the following parameters: $g = -2.0t$, $N_y = 64$, and $5 \leq N_x \leq 32$. We utilize a Chebyshev expansion with 2000 terms, which provides accurate results for our purposes. The Chebyshev BdG algorithm is implemented in C CUDA, a programming language well-suited for parallelization, enabling faster computations. The algorithm was executed on the superLab machines in our laboratory as well as on CETENE's cluster located at the Federal University of Pernambuco (CETENE, 2020).

Figure 13 – Average order parameter $\overline{\Delta}$ versus width (or confinement length) without disorder.

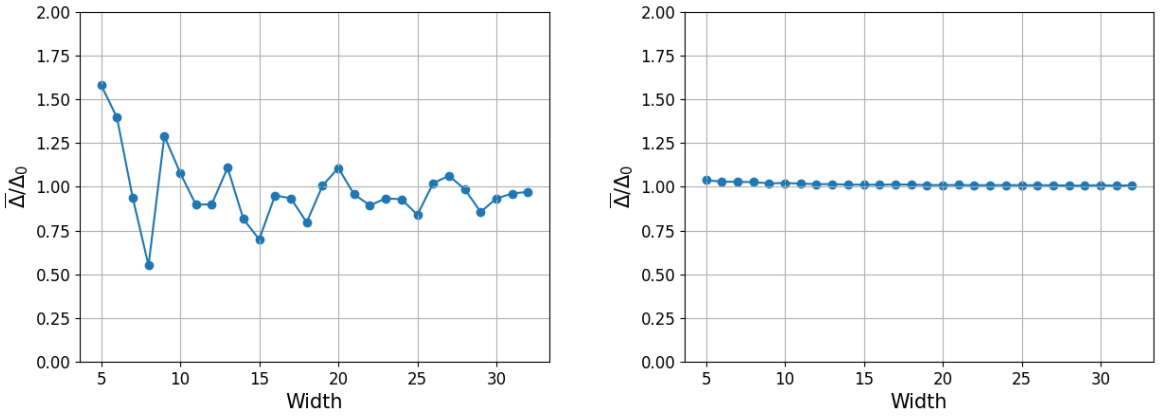

(a) Low density of Electrons $\langle n \rangle = 0.125$.

(b) Mid Density of Electrons $\langle n \rangle = 0.875$

Source: The Author (2023).

We observe two distinct effects on the average order parameter in Figures 13a and 13b, depending on the chosen value of $\langle n \rangle$. Hereafter, we refer to a mid $\langle n \rangle$ as $\langle n \rangle = 0.875$ and a low $\langle n \rangle$ as $\langle n \rangle = 0.125$. For low $\langle n \rangle$, we observe oscillations in the average order parameter as we increase the confinement length. The oscillations tend to dampen as the width increases, and the order parameter tends towards the bulk value, $\Delta_0 = 0.03t$. Conversely, for mid $\langle n \rangle$, the oscillations no longer exist. Instead, the average order parameter becomes insensitive to variations in the confinement length and remains close to its bulk value, $\Delta_0 = 0.35t$. These oscillations can be explained by the Fermi wavelength, which differs from both mid and low $\langle n \rangle$.

By introducing disorder, we can observe how the same scenario changes by altering the correlation degree α and the disorder strength V. In this dissertation, we assign the values $\alpha = 0, 1, 2, 3$ and $V = 0.1t, 0.3t, 0.5t, 0.75t,$ and $1.0t$. Incorporating disorder requires performing several calculations with different random potentials to obtain a reliable average order parameter. To achieve reasonable computational times, we adopt a strategy of reducing the number of samples as the width increases. This approach is motivated by the fact that the

amount of order parameter data increases with the sample size. Consequently, larger samples contain more data than smaller ones, allowing us to achieve comparable results with fewer samples using different random potentials. The number of statistical samples is determined using the following rule: int maxIt = (int) ceil(10000.0/(64*Nx)). Here, maxIt represents the number of samples performed with different potentials. Depending on the confinement length (in this case, Nx), we may have more or fewer samples. The ceil function rounds its argument up to the nearest integer. For instance, ceil(2.5) = 3 and ceil(1.2) = 2. The idea is to choose maxIt as the number of iterations where we have more than 10,000 order parameters to analyze for a given confinement length. This strategy yields reliable statistics and averages, as we will demonstrate further.

5.2 CASE WITH NON-CORRELATED DISORDER

By examining the plotted graphs with mid $\langle n \rangle$, 14b, interesting insights can be gleaned regarding the influence of disorder strength on the order parameter. Initially, at low disorder magnitudes, the order parameter shows limited sensitivity to the presence of disorder. However, as the disorder strength increases, the order parameter progressively decreases, indicating a suppression of superconductivity at intermediate order parameter values. It should be noted that investigations into high disorder strengths have not yet been conducted, but it is expected that further increases in disorder would cause the order parameter to rise again, similar to what is observed in unconstrained samples.

Nevertheless, it is crucial to not only consider the behavior of the order parameter but also examine the probability of encountering a zero order parameter. This is because an increase in disorder does not lead to the enhancement of a homogeneous order parameter.

Hence, it can be inferred that the order parameter diminishes with increasing disorder strength, but further disorder escalation prompts its resurgence. These observations align with the findings obtained from bulk samples, as documented by Gastiosoro (GASTIASORO; ANDERSEN, 2018) and Neverov (NEVEROV et al., 2022).

Now let us consider the situation of low $\langle n \rangle$, shown in Figure 14a. In this specific case, even though there is no upper limit on the Debye window, the effects of quantum size in superconductivity become clearly evident. This can be attributed to the confinement of the Debye window to the lower boundary of the conduction band. The impact of disorder on these observations is particularly noteworthy and becomes immediately apparent. As we increase the

Figure 14 – Average order parameter $\overline{\Delta}$ versus width for $\alpha = 0$.

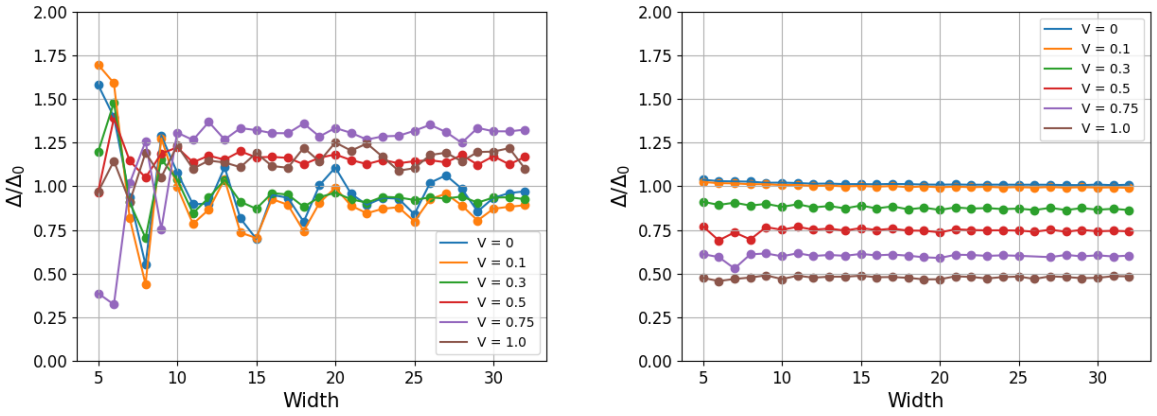

(a) Low $\langle n \rangle$ (b) Mid $\langle n \rangle$

Source: The Author (2023).

strength of disorder, we observe a suppression of quantum-size oscillations. Moreover, when the disorder strength reaches a value of 1, these oscillations are completely halted for samples with an average confinement. It is worth highlighting that in cases of strong confinement, especially for smaller transverse wire sizes, increasing disorder gradually replaces the enhancement of superconductivity due to quantum-well effects with its suppression.

5.3 CASE WITH CORRELATED DISORDER

Figure 15 – Average order parameter $\overline{\Delta}$ versus width for V $= 0.1$t.

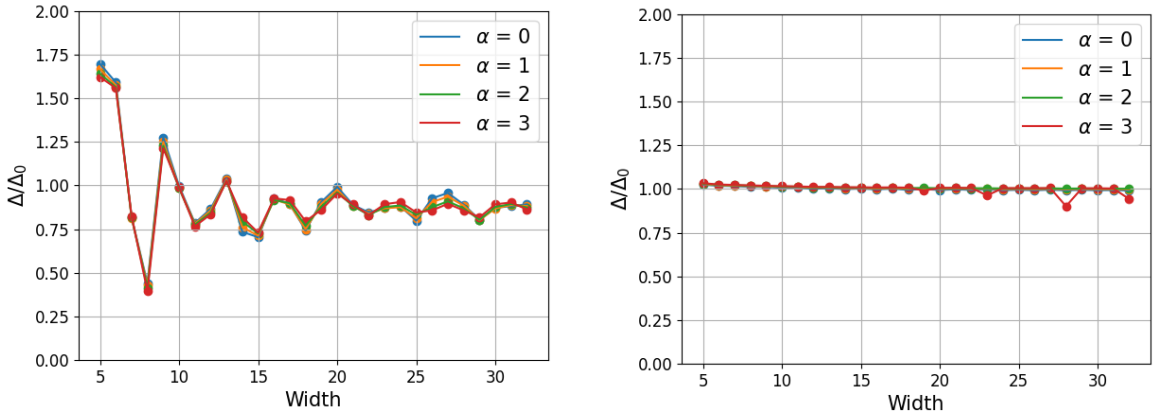

(a) $\langle n \rangle = 0.125$ (b) $\langle n \rangle = 0.875$

Source: The Author (2023).

In Figures 15, 16, 17, 18 and 19 we can observe distinct behaviors of the average order

Figure 16 – Average order parameter $\overline{\Delta}$ versus width for V = 0.3t.

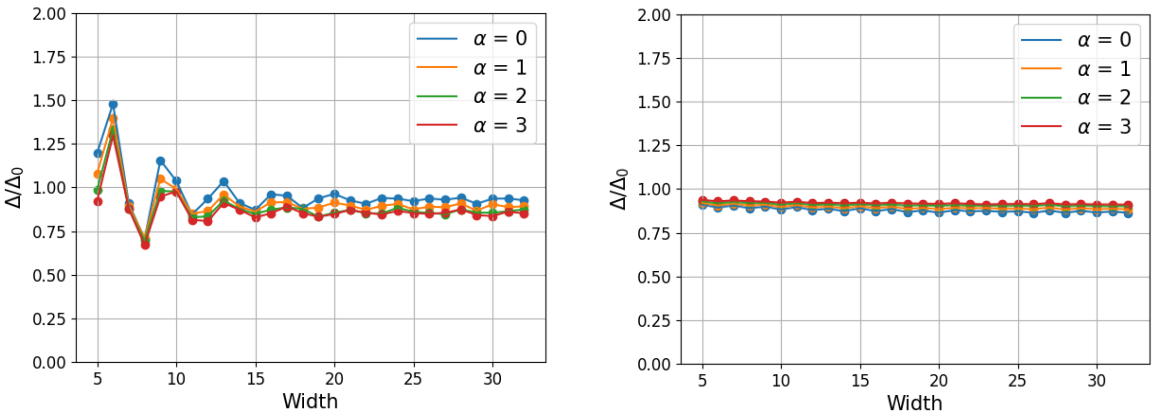

(a) $\langle n \rangle = 0.125$ (b) $\langle n \rangle = 0.875$

Source: The Author (2023).

Figure 17 – Average order parameter $\overline{\Delta}$ versus width for V = 0.5t.

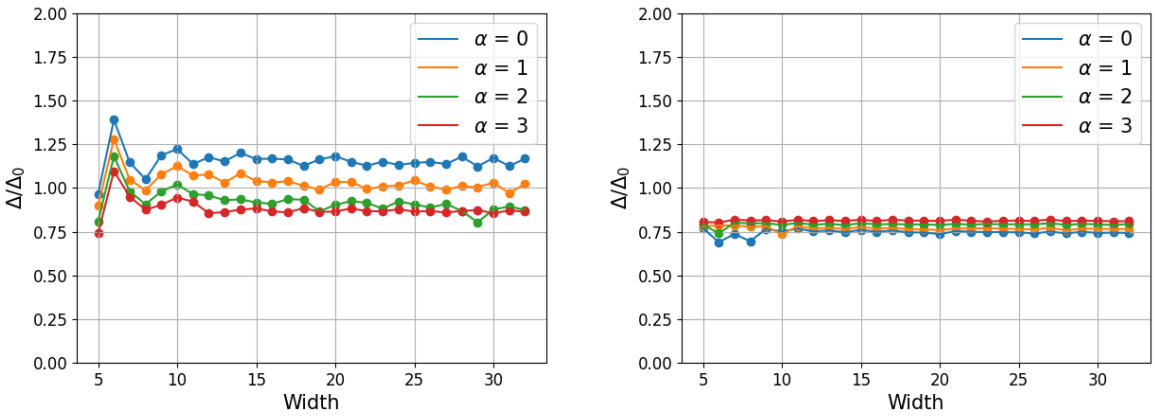

(a) $\langle n \rangle = 0.125$ (b) $\langle n \rangle = 0.875$

Source: The Author (2023).

parameter as we vary the parameters V, α, and the width of the nanowire. Specifically, for mid $\langle n \rangle$, the system appears to be insensitive to changes in the nanowire width, while for low $\langle n \rangle$, the oscillations continue to evolve with increasing width.

The effects of V and α are also noteworthy. Increasing V leads to the smoothing of oscillations for widths exceeding 10 length units. On the other hand, increasing α causes the order parameter value for larger widths to approach different values. Similar trends are observed in the case of mid $\langle n \rangle$ when V and α are increased. Although no oscillations are present, the approach to the limiting value for larger widths still exhibits sensitivity to changes in α.

One significant difference between the results lies in the behavior of the order parameter with respect to V. For mid $\langle n \rangle$, the order parameter tends to decrease as V increases. However,

Figure 18 – Average order parameter $\overline{\Delta}$ versus width for V = 0.75t.

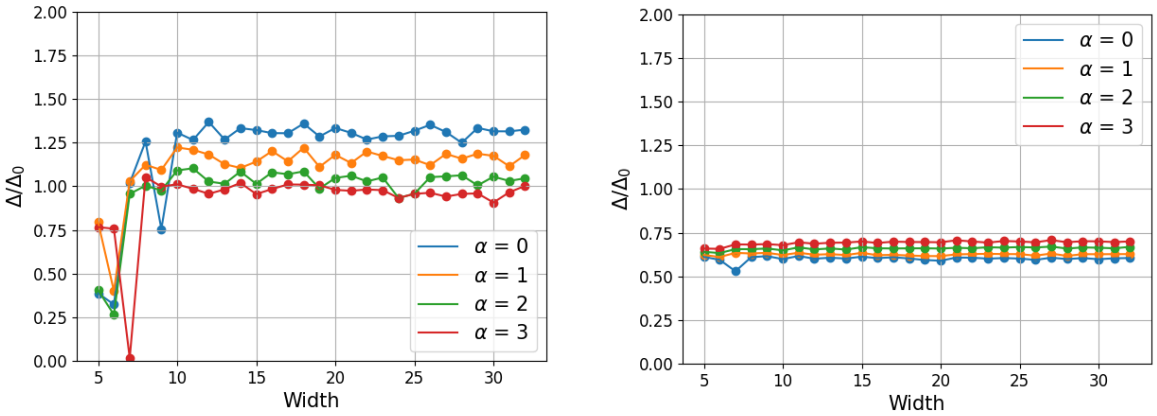

(a) $\langle n \rangle = 0.125$ (b) $\langle n \rangle = 0.875$

Source: The Author (2023).

Figure 19 – Average order parameter $\overline{\Delta}$ versus width for V = 1.0t.

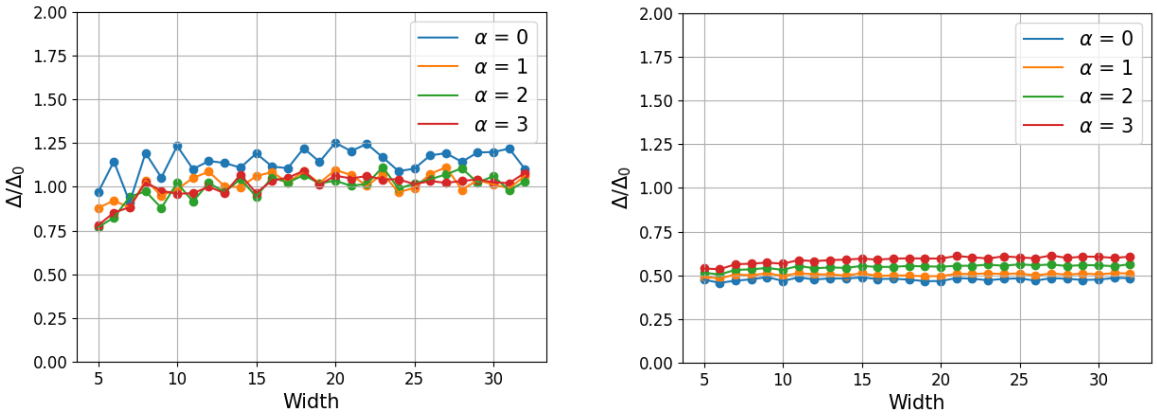

(a) $\langle n \rangle = 0.125$ (b) $\langle n \rangle = 0.875$

Source: The Author (2023).

for low $\langle n \rangle$, we observe an increase in the average value for $V = 0.75t$ until it approaches the bulk value again at $V = 1.0t$. At $V = 1.0t$, the oscillations are significantly suppressed, and the plots for different α values tend to overlap, indicating a convergence towards a common limiting value. Nevertheless, the evolution of the system with increasing width exhibits a peculiar mixing behavior.

The histograms for the order parameter also exhibit variations. Specifically, it can be observed that for low $\langle n \rangle$, the strength of the oscillations is more pronounced for smaller values of the confinement length, resulting in different histogram shapes. To illustrate this, we present the histograms corresponding to confinement lengths ranging from 5 to 9 for low $\langle n \rangle$.

Figure 20 – Histogram of Order Parameter for sample with size: 5x64.

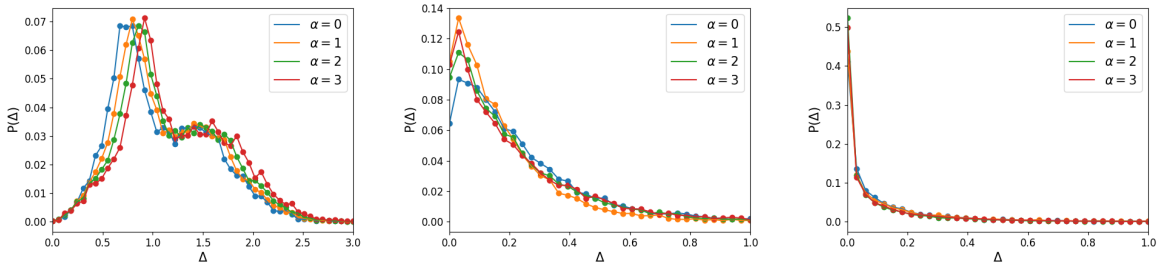

(a) V = 0.1t $\langle n \rangle = 0.125$ (b) V = 0.5t $\langle n \rangle = 0.125$ (c) V = 1.0t $\langle n \rangle = 0.125$

Source: The Author (2023).

Figure 21 – Histogram of Order Parameter for sample with size: 6x64.

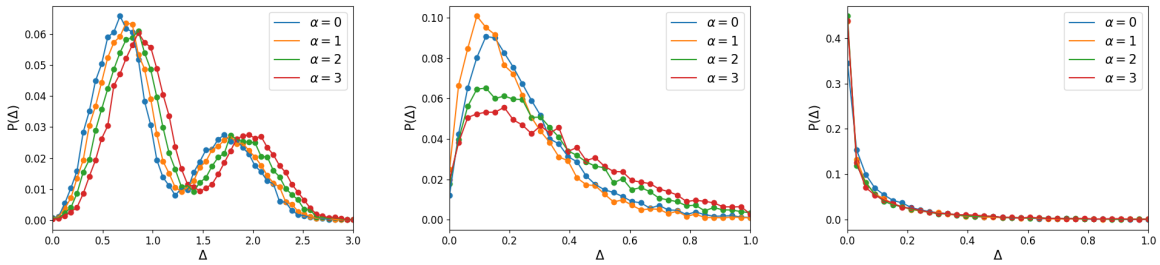

(a) V = 0.1t $\langle n \rangle = 0.125$ (b) V = 0.5t $\langle n \rangle = 0.125$ (c) V = 1.0t $\langle n \rangle = 0.125$

Source: The Author (2023).

Figure 22 – Histogram of Order Parameter for sample with size: 7x64.

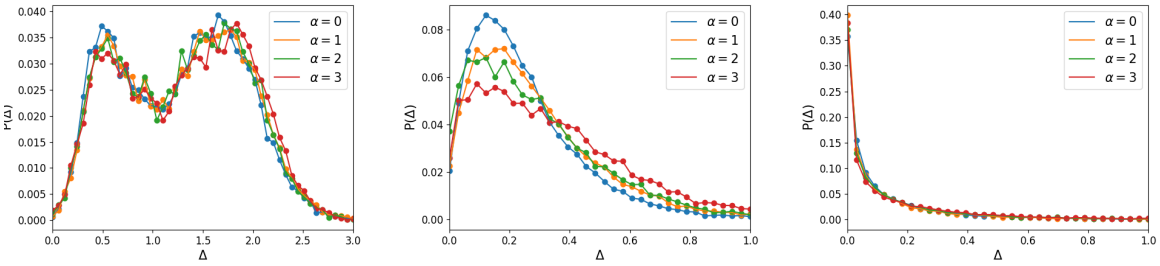

(a) V = 0.1t $\langle n \rangle = 0.125$ (b) V = 0.5t $\langle n \rangle = 0.125$ (c) V = 1.0t $\langle n \rangle = 0.125$

Source: The Author (2023).

The histograms, which capture the stronger oscillations, are depicted in Figures 20, 21, 22, 23 and 24.

The shape of the distribution undergoes significant changes for small confinement lengths, but as the confinement length increases, all plots tend to exhibit similar distributions, which primarily depend on the disorder strength. Increasing the confinement length leads to a spread and closer approach to the value $\Delta_i = 0$, influenced by the disorder strength. This implies

Figure 23 – Histogram of Order Parameter for sample with size: 8x64.

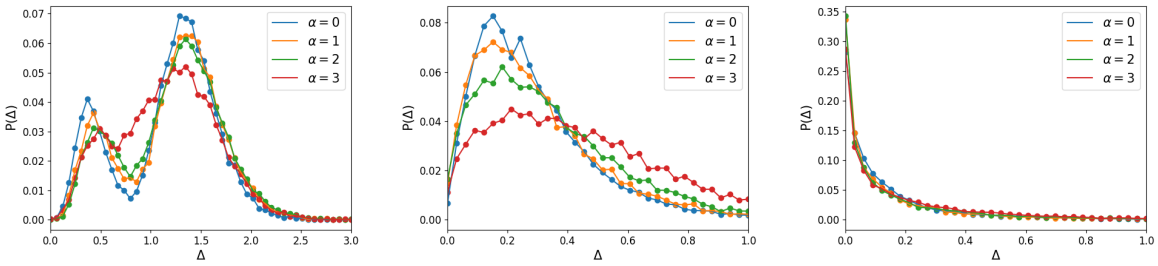

(a) V = 0.1t $\langle n \rangle = 0.125$ (b) V = 0.5t $\langle n \rangle = 0.125$ (c) V = 1.0t $\langle n \rangle = 0.125$

Source: The Author (2023).

Figure 24 – Histogram of Order Parameter for sample with size: 9x64.

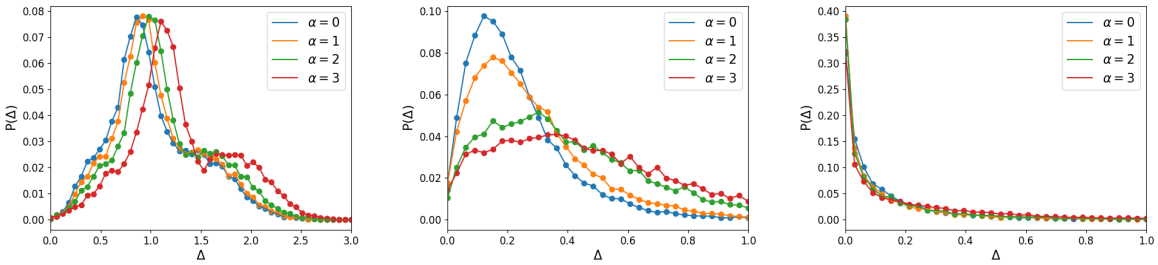

(a) V = 0.1t $\langle n \rangle = 0.125$ (b) V = 0.5t $\langle n \rangle = 0.125$ (c) V = 1.0t $\langle n \rangle = 0.125$

Source: The Author (2023).

Figure 25 – Histogram of Order Parameter for sample with size: 5x64.

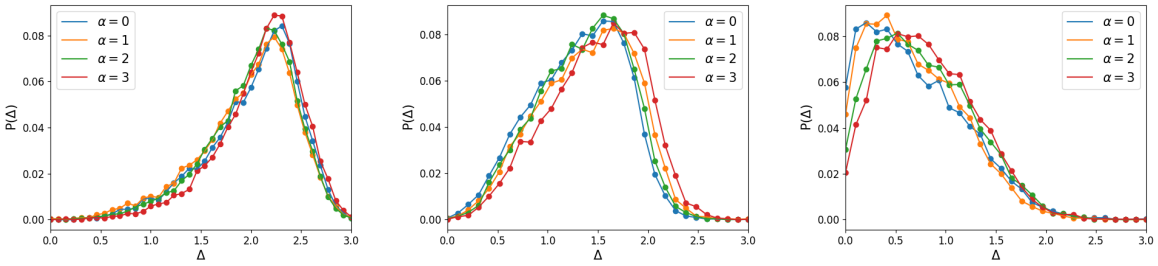

(a) V = 0.1t $\langle n \rangle = 0.875$ (b) V = 0.5t $\langle n \rangle = 0.875$ (c) V = 1.0t $\langle n \rangle = 0.875$

The Author (2023).

that several values of the order parameter tend to approach zero, although the tail of the distribution decreases slowly enough to prevent the average Δ_i from being close to zero, as depicted in Figure 5.2.

In the case of mid $\langle n \rangle$, a distinct behavior is observed. The histograms for the order parameter appear to be insensitive to changes in the confinement length, as evidenced in Figures 25, 26, 27, 28 and 29.

Figure 26 – Histogram of Order Parameter for sample with size: 6x64.

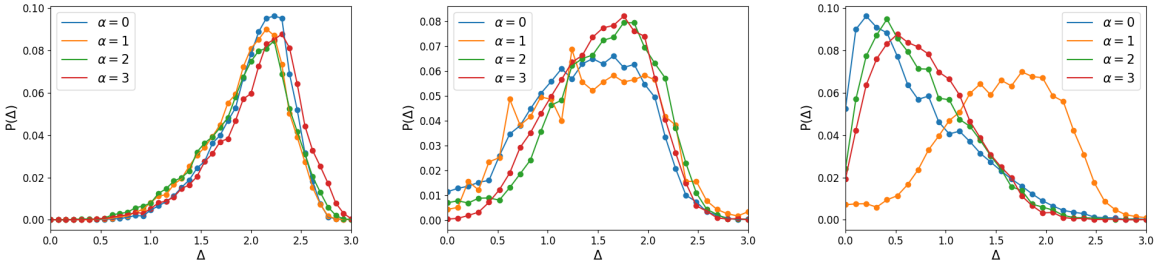

(a) V = 0.1t $\langle n \rangle = 0.875$ (b) V = 0.5t $\langle n \rangle = 0.875$ (c) V = 1.0t $\langle n \rangle = 0.875$

Source: The Author (2023).

Figure 27 – Histogram of Order Parameter for sample with size: 7x64.

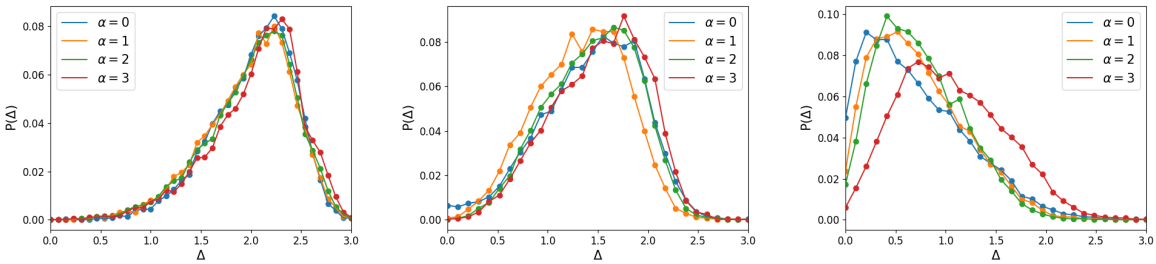

(a) V = 0.1t $\langle n \rangle = 0.875$ (b) V = 0.5t $\langle n \rangle = 0.875$ (c) V = 1.0t $\langle n \rangle = 0.875$

Source: The Author (2023).

Figure 28 – Histogram of Order Parameter for sample with size: 8x64.

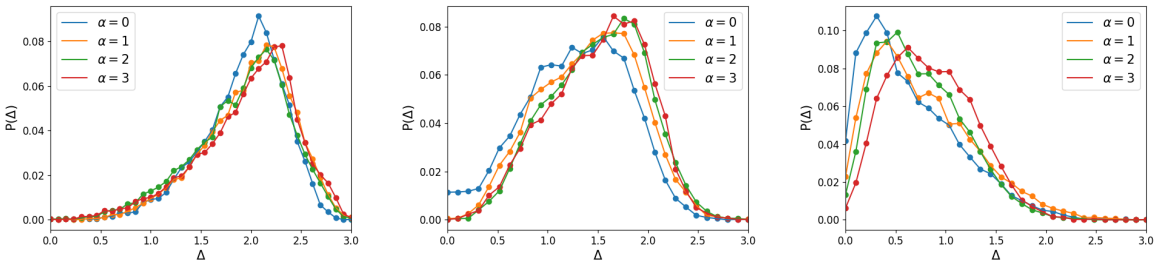

(a) V = 0.1t $\langle n \rangle = 0.875$ (b) V = 0.5t $\langle n \rangle = 0.875$ (c) V = 1.0t $\langle n \rangle = 0.875$

Source: The Author (2023).

Figure 29 – Histogram of Order Parameter for sample with size: 9x64.

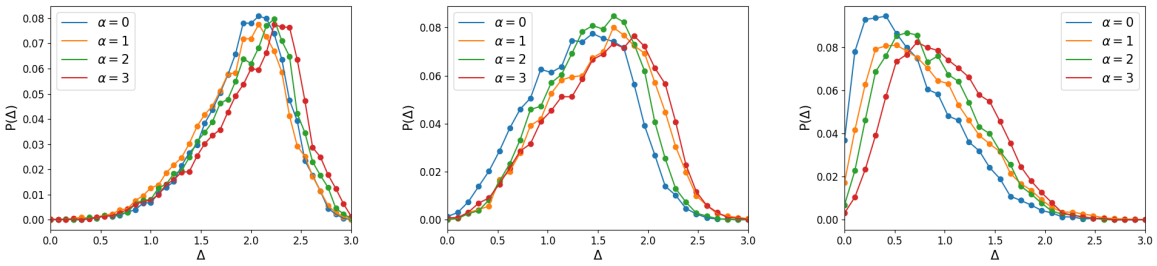

(a) V = 0.1t $\langle n \rangle = 0.875$ (b) V = 0.5t $\langle n \rangle = 0.875$ (c) V = 1.0t $\langle n \rangle = 0.875$

Source: The Author (2023).

The introduction of disorder with varying strength and correlation degree leads to a decrease in the average order parameter and a splitting of the approaching value into multiple distinct values, consistent with the qualitative findings in Chapter 4.4. Furthermore, the shape of the distributions exhibits remarkable similarity for disorder strengths of V = 0.1t, 0.5t, and 1.0t. Interestingly, the presence of a confinement length does not appear to have any noticeable impact on the statistical properties of the order parameter when comparing mid $\langle n \rangle$ under quasi-1D samples and periodic boundary conditions.

As we approach large confinement values, the system reaches a stationary distribution that remains unchanged as the confinement length increases. Figures 30, 31, 32, 33 and 34 presents the distributions for the largest calculated confinement, 64x32, for both mid and low $\langle n \rangle$. For slightly smaller confinement values, no further evolution in the histogram shape was observed beyond what is depicted in the figure. Notably, low $\langle n \rangle$ samples exhibit greater sensitivity to disorder compared to mid $\langle n \rangle$ samples. This is evident from the figure, as the same amount of disorder moves the histogram closer to zero Δ_i in low $\langle n \rangle$ samples, while in mid $\langle n \rangle$ samples, although there is a slight shift towards the left, the most probable value remains far from zero.

Figure 30 – Histogram of Order Parameter for sample with size 32x64 for V = 0.1t.

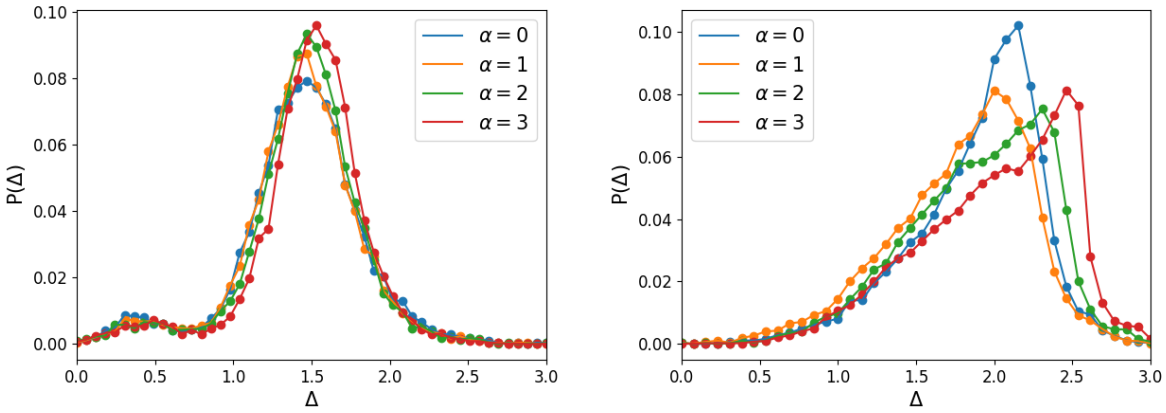

(a) $\langle n \rangle = 0.125$ (b) $\langle n \rangle = 0.875$

Source: The Author (2023).

Figure 31 – Histogram of Order Parameter for sample with size 32x64 for V = 0.3t.

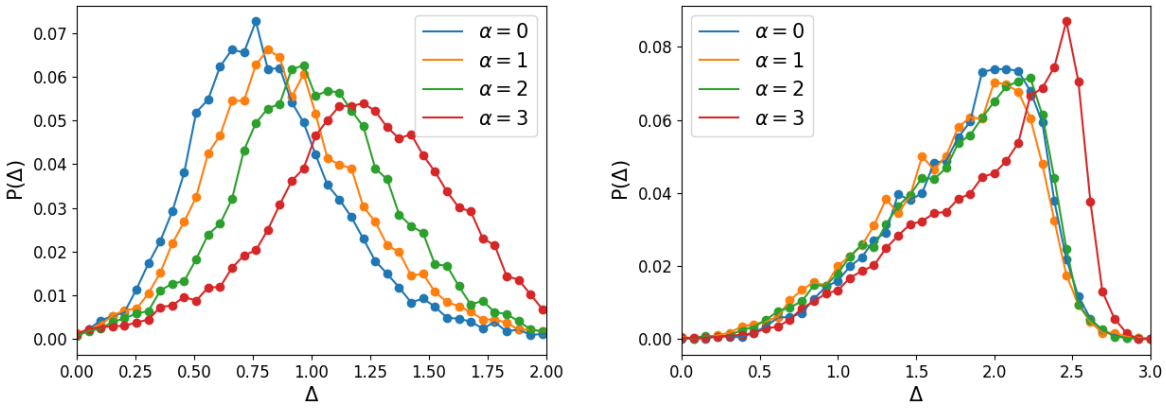

(a) $\langle n \rangle = 0.125$ (b) $\langle n \rangle = 0.875$

Source: The Author (2023).

Figure 32 – Histogram of Order Parameter for sample with size 32x64 for V = 0.5t.

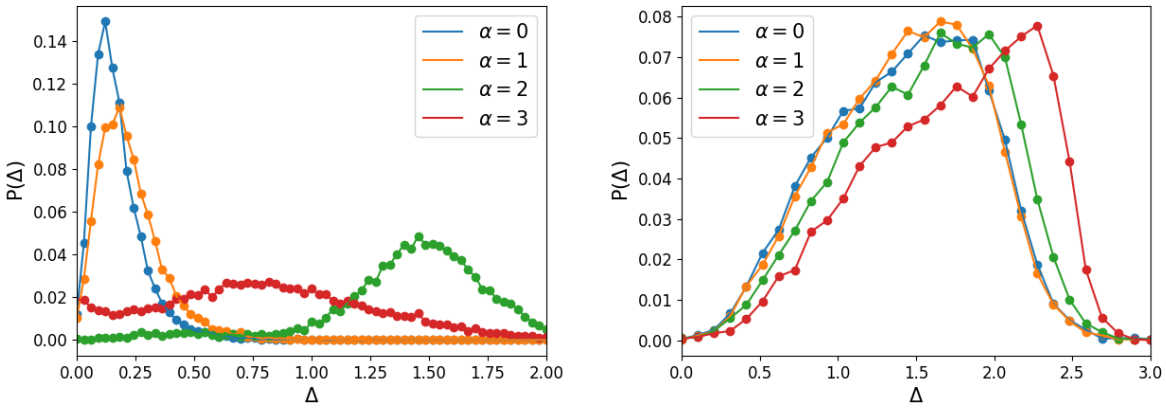

(a) $\langle n \rangle = 0.125$ (b) $\langle n \rangle = 0.875$

Source: The Author (2023).

Figure 33 – Histogram of Order Parameter for sample with size 32x64 for V = 0.75t.

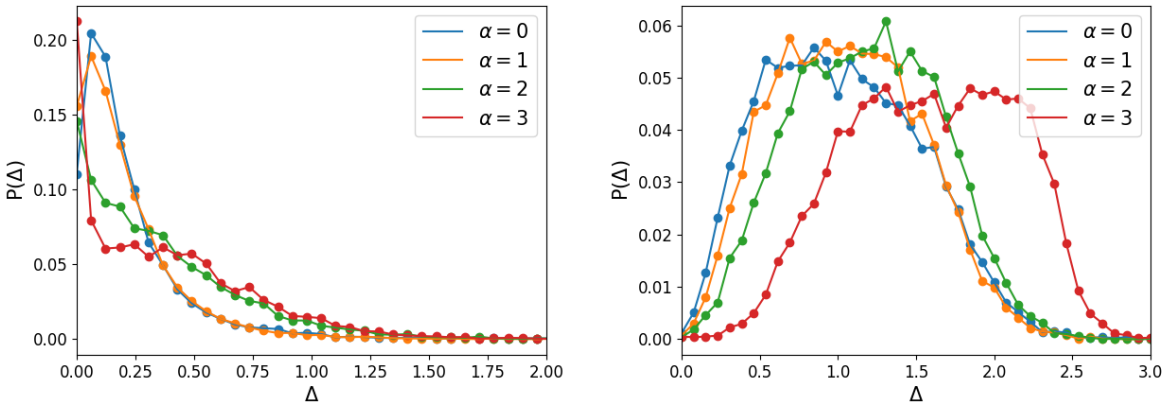

(a) $\langle n \rangle = 0.125$ (b) $\langle n \rangle = 0.875$

Source: The Author (2023).

Figure 34 – Histogram of Order Parameter for sample with size 32x64 for V = 1.0t.

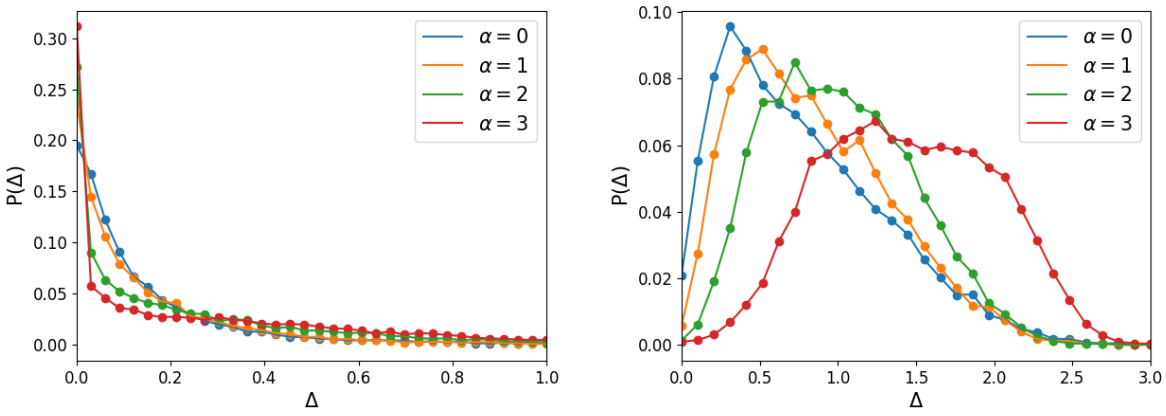

(a) $\langle n \rangle = 0.125$ (b) $\langle n \rangle = 0.875$

Source: The Author (2023).

6 CONCLUSION

The findings of this work are as follows:

- The dependence of the order parameter (OP) on the transverse dimensions of the sample is significantly influenced by the electron density. The quantum-size effect is suppressed as the Fermi level approaches the middle of the conduction band (mid-band).
- The effect of disorder on the superconducting properties strongly depends on the electron density of the material. For electron density corresponding to the mid-band, the effect is much weaker compared to when the Fermi level is located in the vicinity of the band edges.
- In the case of large electron density, decreasing the size of a pure sample leads to a weak monotonic correlation-dependent increase in the average OP. The situation is reversed in the case of a dirty sample.
- For low electron density, as expected, reducing the size of a pure sample leads to a strong non-monotonic correlation-dependent increase in the average OP. Increasing disorder in a dirty sample results in a significant suppression of superconductivity with decreasing transverse dimensions.
- For low electron density we have seen an increase in order parameter for increases of disorder in a certain range.

All of these observations manifest as changes in the spatial profile, statistical distribution, and spatial correlations of the order parameter, and are dependent on the sample size.

This work highlights the significant impact of correlations on superconductivity in quasi-low dimensional materials and structures, rendering it more robust and less sensitive to disorder potential. Consequently, the superconducting properties in such materials and structures can be controlled not only by the total density of impurities and defects but also by their spatial correlations.

Our study is relevant because very few currently is known about correlated disorder in superconductors, and we are able to show in this dissertation few caracteristics of the effect of correlation disorder in quasi-1D samples by increasing the confinement length.

For future perspectives we intend to continue calculations for bigger disorder and correlation parameter. We also intend to calculate superfluid stiffness, a more accurate criteria for superconductivity than the order parameter.

REFERENCES

ANDERSON, P. Superconductivity: the implications of the meissner effect. *Journal of Physics and Chemistry of Solids*, Elsevier, v. 11, n. 1-2, p. 26–30, 1959. Disponível em: <https://www.sciencedirect.com/science/article/abs/pii/0022369759900368?via%3Dihub>.

BARDEEN, J.; COOPER, L. N.; SCHRIEFFER, J. R. Theory of superconductivity. *Phys. Rev.*, American Physical Society, v. 108, p. 1175–1204, Dec 1957. Disponível em: <https://link.aps.org/doi/10.1103/PhysRev.108.1175>.

BLATT, J. M.; THOMPSON, C. J. Shape resonances in superconducting thin films. *Phys. Rev. Lett.*, American Physical Society, v. 10, p. 332–334, Apr 1963. Disponível em: <https://link.aps.org/doi/10.1103/PhysRevLett.10.332>.

BRUUS, H.; FLENSBERG, K. *Many-Body Quantum Theory in Condensed Matter Physics: An Introduction (Oxford Graduate Texts)*. Hardcover. [S.l.]: Oxford University Press, 2004. 435 p. ISBN 0198566336.

CETENE. *CETENE Cluster Website*. 2020. <https://antigo.cetene.gov.br/cluster>. Accessed on: January 10, 2022.

COSTA, M. B. S.; PAVãO, A. C. Supercondutividade: um século de desafios e superação. *Revista Brasileira de Ensino de Física*, v. 34, n. 2, p. 2505, 2012. Disponível em: <https://doi.org/10.1590/S1806-11172012000200017>.

COVACI, L.; PEETERS, F. M.; BERCIU, M. Efficient numerical approach to inhomogeneous superconductivity: The chebyshev-bogoliubov–de gennes method. *Phys. Rev. Lett.*, American Physical Society, v. 105, p. 167006, Oct 2010. Disponível em: <https://link.aps.org/doi/10.1103/PhysRevLett.105.167006>.

CROITORU, M.; SHANENKO, A.; PEETERS, F. Size-resonance effect in cylindrical superconducting nanowire. *Moldavian Journal of the Physical Sciences*, v. 6, n. 1, 2007.

DROZDOV, A. P.; KONG, P. P.; MINKOV, V. S.; BESEDIN, S. P.; KUZOVNIKOV, M. A.; MOZAFFARI, S.; BALICAS, L.; BALAKIREV, F. F.; GRAF, D. E.; PRAKAPENKA, V. B.; GREENBERG, E.; KNYAZEV, D. A.; TKACZ, M.; EREMETS, M. I. Superconductivity at 250 k in lanthanum hydride under high pressures. *Nature*, v. 569, n. 7757, p. 528–531, 2019. ISSN 0028-0836. Disponível em: <https://doi.org/10.1038/s41586-019-1201-8>.

FEDER, J. *Fractals*. New York, NY: Plenum Press, 1988. ISBN 978-0306423074.

GASTIASORO, M. N.; ANDERSEN, B. M. Enhancing superconductivity by disorder. *Physical Review B*, v. 98, n. 18, p. 184510, 2018.

GENNES, P.-G. de. *Superconductivity of Metals and Alloys*. 1st. ed. Boulder, CO: Westview Press, 1999. ISBN 978-0738203151.

GHOSAL, A.; RANDERIA, M.; TRIVEDI, N. Inhomogeneous pairing in highly disordered s-wave superconductors. *Phys. Rev. B*, American Physical Society, v. 65, p. 014501, Nov 2001. Disponível em: <https://link.aps.org/doi/10.1103/PhysRevB.65.014501>.

HASSANI, S. *Mathematical Physics: A Modern Introduction to Its Foundations*. 2nd. ed. New York, NY: Springer, 2013.

IEEE. *Nobel Laureates Superconductivity*. 2022. <http://past.ieeecsc.org/pages/nobel-laureates-superconductivity>. Accessed on: June 23, 2023.

KITTEL, C. *Introduction to Solid State Physics*. 8. ed. Wiley, 2004. ISBN 9780471415268. Disponível em: <http://www.amazon.com/Introduction-Solid-Physics-Charles-Kittel/dp/047141526X/ref=dp_ob_title_bk>.

MANDELBROT, B. B. *The Fractal Geometry of Nature*. 1st. ed. New York: W. H. Freeman and Company, 1982.

MOURA, F. A. B. F. de; LYRA, M. L. Delocalization in the 1d anderson model with long-range correlated disorder. *Phys. Rev. Lett.*, American Physical Society, v. 81, p. 3735–3738, Oct 1998. Disponível em: <https://link.aps.org/doi/10.1103/PhysRevLett.81.3735>.

NAGAI, Y.; OTA, Y.; MACHIDA, M. Efficient numerical self-consistent mean-field approach for fermionic many-body systems by polynomial expansion on spectral density. *Journal of the Physical Society of Japan*, v. 81, n. 2, p. 024710, 2012. Disponível em: <https://doi.org/10.1143/JPSJ.81.024710>.

NEVEROV, V. D.; LUKYANOV, A. E.; KRASAVIN, A. V.; VAGOV, A.; CROITORU, M. D. Correlated disorder as a way towards robust superconductivity. *Communications Physics*, v. 5, n. 1, p. 177, 2022. ISSN 2399-3650. Disponível em: <https://doi.org/10.1038/s42005-022-00933-z>.

OREG, Y. *Concepts in Condensed Matter Physics: Tutorial I - Tight Binding and The Hubbard Model*. 2018. <https://www.weizmann.ac.il/condmat/oreg/sites/condmat.oreg/files/uploads/2018/tutorial1.pdf>. Accessed on: December 16, 2021.

PENG, J.; YU, Z.; WU, J.; ZHOU, Y.; GUO, Y.; LI, Z.; ZHAO, J.; WU, C.; XIE, Y. Title of the article. *ACS Nano*, v. 12, p. 9461, 2018.

PETROVIC, A. P.; ANSERMET, D.; CHERNYSHOV, D.; HOESCH, M.; SALLOUM, D.; GOUGEON, P.; POTEL, M.; BOERI, L.; PANAGOPOULOS, C. Title of the article. *Nature Communications*, v. 7, p. 12262, 2016.

SCHILLING, A.; CANTONI, M.; GUO, J. D.; OTT, H. R. Superconductivity in the hg-ba-ca-cu-o system. *Nature*, v. 363, n. 6424, p. 56–58, 1993. ISSN 0028-0836. Disponível em: <https://doi.org/10.1038/363056a0>.

TANAKA, H.; KUNISHIMA, W.; ITOH, M. Riken rev. v. 29, p. 20, 2000.

TINKHAM, M. *Introduction to Superconductivity*. Mineola, NY: Dover Publications, 2004. ISBN 978-0486435039.

XIANG, T.; WU, C. *D-wave Superconductivity*. [S.l.]: Cambridge University Press, 2022.

ZHU, J.-X. *Bogoliubov-de Gennes Method and Its Applications*. 1. ed. [S.l.]: Springer Cham, 2016. XI, 188 p. (Lecture Notes in Physics). Softcover ISBN: 978-3-319-31312-2, eBook ISBN: 978-3-319-31314-6.